Chapter 5
The Ribbon Synapse Between Type I Spiral Ganglion Neurons and Inner Hair Cells

Mark A. Rutherford and Tobias Moser

Keywords Action potential generation · Active zone · Cochlea · Exocytosis · Glutamate receptor · Nanodomain · Synaptic heterogeneity · Synaptic ribbon · Synaptic vesicle · Voltage-gated calcium channel $Ca_v1.3$

5.1 Introduction

5.1.1 Overview

Sound pressure waves induce vibrations in the cochlea that produce graded receptor potentials in presynaptic sensory inner hair cells (IHCs). Ultimately, sounds are represented in the output of the cochlea by patterns of action potentials (APs) in spiral ganglion neurons (SGNs). These APs travel to the brain along the afferent fibers of the auditory nerve, which are myelinated axons of SGNs. This transformation of vibrations to electrical impulses is an analog-to-digital conversion taking place in the organ of Corti. Information about acoustic stimuli is encoded through IHC–SGN synaptic transmission and subsequent AP generation in the postsynaptic SGN.

M.A. Rutherford (✉)
Department of Otolaryngology, Central Institute for the Deaf, Washington University School of Medicine, 660 South Euclid Ave, St. Louis, MO 63110, USA
e-mail: rutherfordm@ent.wustl.edu

T. Moser (✉)
Institute for Auditory Neuroscience and Inner Ear Lab, Collaborative Research Center 889, University Medical Center Göttingen, Robert-Kochstr. 40, 37075 Göttingen, Germany
e-mail: tmoser@gwdg.de

A. Dabdoub et al. (eds.), *The Primary Auditory Neurons of the Mammalian Cochlea*, Springer Handbook of Auditory Research 52,
DOI 10.1007/978-1-4939-3031-9_5

5.1.2 The Type I Spiral Ganglion Neuron

The peripheral connectivity of type I SGNs, from the spiral ganglion to the organ of Corti, is shown for one tonotopic position in Fig. 5.1. Tonotopy determines the frequency of maximum sensitivity. Moreover, the APs in each type I SGN contain information about temporal dynamics and sound level in their precise timing and mean rate. The synapses between cochlear outer hair cells and type II SGNs are not covered in this chapter; therefore we will refer to type I SGNs simply as SGNs.

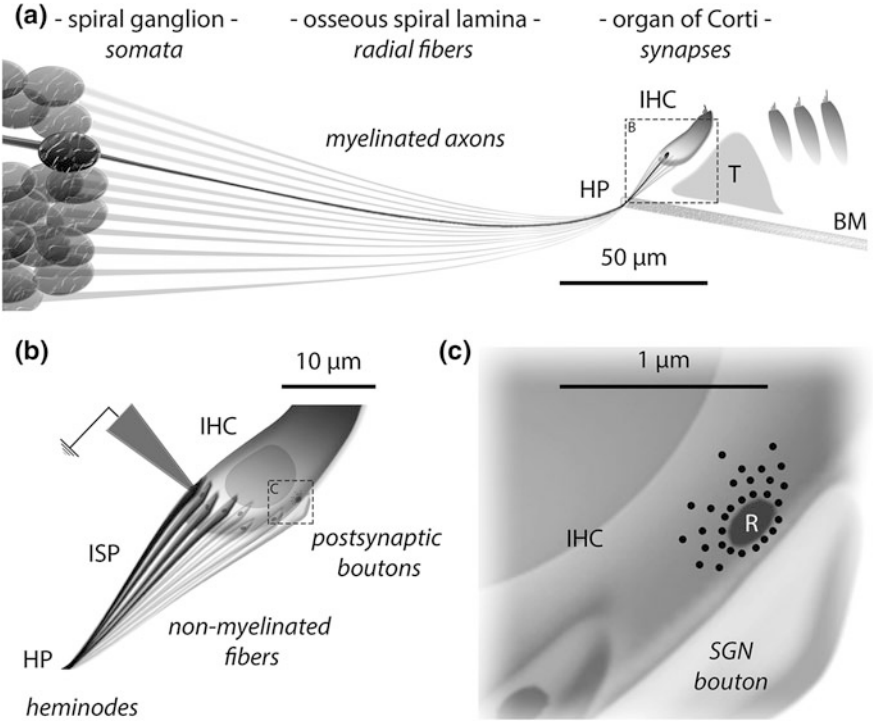

Fig. 5.1 Radial section schematic of spiral ganglion neurons in the cochlea. **a** The spiral ganglion is on *left*, showing several somas of type I spiral ganglion neurons (*SGNs*) all connected to one inner hair cell (*IHC*) in the organ of Corti on *right*, each via a single myelinated axon called a radial fiber. The radial fibers go through habenulas perforata (*HP*) to reach the neuropil of the inner spiral plexus (*ISP*) underneath IHCs in the organ of Corti. See *boxed* region enlarged in **b**. T, tunnel of Corti; BM, basilar membrane. One SGN is highlighted in *black*. *SGN anatomical parts* are labeled in *italic font*. **b** Synaptic transmission initiates a postsynaptic depolarization in the bouton and nonmyelinated fiber that triggers an action potential (*AP*) at the heminode near the HP (Sect. 5.4.4). An AP then propagates along the peripheral myelinated axon **a** via nodes of Ranvier to the soma in the spiral ganglion, then along the centrally projecting axon (not shown). **c** Each SGN receives excitatory synaptic input via one IHC presynaptic active zone, marked by a presynaptic ribbon (*R*), and surrounded by synaptic vesicles. (Modified from Rutherford et al., 2012). Spike encoding of neurotransmitter release timing by spiral ganglion neurons of the cochlea. *The Journal of Neuroscience*, 32(14), 4773–4789)

Starting from the periphery, in the organ of Corti, each SGN contacts a single synapse on one IHC via a single postsynaptic bouton (Fig. 5.1). The bouton is connected to the soma via the SGN's short nonmyelinated segment and longer peripheral myelinated axon. Beyond the SGN soma in the spiral ganglion, the myelinated central axon projects to the brain stem (see Muniak et al., Chap. 6).

As the SGN fiber exits the organ of Corti into the osseous spiral lamina, the cable thickens and the myelin begins just beyond the habenula perforata (HP; Fig. 5.1a, b). APs are likely initiated there, relatively near the IHC–SGN synapses in the neuropil of the inner spiral plexus (ISP; Fig. 5.1b). In the neuropil environment of the ISP between bouton and HP, the SGN fiber is surrounded by other afferent fibers, presynaptic terminals of efferent fibers, and nonneuronal glia-like supporting cells. It is unclear whether this part of the SGN should be called a nonmyelinated axon or a dendrite. The great majority of SGN fibers do not branch (Liberman, 1980). Therefore, in general AP generation in each SGN depends on excitatory input to its postsynaptic bouton from a single presynaptic ribbon-type active zone (AZ) of one IHC (Fig. 5.1c).

5.1.3 The Inner Hair Cell

IHCs are the primary sensory receptors in the organ of Corti. They mediate mechanotransduction through the hair bundle comprised of stereocilia. Ionic current through the bundle drives the receptor potential continuously, depolarizing the IHC to modulate the opening of voltage-gated Ca^{2+} channels at synapses. IHCs release glutamate at rest and in response to sound, initiating the postsynaptic depolarization that generates spontaneous and evoked APs in SGNs. Each IHC excites multiple SGNs. For example, cochleae of mammals such as mice and rats have around 1000 IHCs and approximately 20,000 SGNs.

In murine species and other mammals as well, the number of SGNs per IHC varies tonotopically (Spoendlin, 1972; Bohne et al., 1982). As illustrated in Fig. 5.1, in the developed ears of cats and mice, for example, each SGN is excited by a single ribbon-type AZ (i.e., a single ribbon synapse on one IHC). Therefore, like the number of SGNs, the number of ribbon synapses per IHC varies tonotopically (Meyer et al., 2009). In general, there are fewer than 10 afferent synapses per IHC in the extreme cochlear base and apex, and 15–30 synapses per IHC in the mid-cochlea. Greater synaptic density correlates with greater hearing acuity for mid-cochlear frequencies. For example, the tonotopic location of peak innervation density corresponds to frequencies of peak behavioral sensitivity (Ehret, 1976).

The 1:1 connection between ribbon synapse and SGN means that each IHC AZ provides the sole excitatory input to its SGN. In this way, each IHC AZ has one private line of communication from ear to brain. The specific sound-response properties of these communication lines differ from each other, depending greatly on mechanisms inherent to the given IHC AZ and its paired SGN. Through these

heterogeneous synaptic connections, information diverges from one IHC receptor potential to multiple SGNs with different response properties (Sect. 5.5).

5.1.4 The IHC Ribbon-Type Active Zone

The presynaptic AZ of each afferent synapse is occupied by a synaptic ribbon, a vesicle-tethering presynaptic electron-dense structural hallmark of the IHC–SGN synapse (Smith & Sjöstrand, 1961). Synaptic ribbons, found in cell types that release transmitter in response to graded stimulus-evoked receptor potentials, are composed predominantly of Ribeye (Schmitz et al., 2000; Khimich et al., 2005), a protein with both an enzymatic function (Schwarz et al., 2011) and an aggregating property thought to bind the ribbon together (Magupalli et al., 2008). Each synaptic ribbon has tens of vesicles tethered to it, a fraction of which are also tethered to the plasma membrane of the AZ (Frank et al., 2010). Structurally and molecularly, synaptic ribbons seem to be exocytosis nanomachines (Lenzi & von Gersdorff, 2001; Rutherford & Pangršič, 2012). One hypothesis is that ribbons inexhaustibly support high rates of transmitter release at continuously active sensory synapses by promoting the association of Ca^{2+} channels with fusion-competent vesicles. However, the complete functions of synaptic ribbons in IHC–SGN sensory encoding remain incompletely understood.

Ribbon-type AZs are large relative to AZs in the brain. Relative to each other, the ribbon-type AZs of hair cells exhibit marked heterogeneity in size. Putatively, differences in AZ size and protein content significantly influence AZ function (Sect. 5.5). In the absence of sound, different SGNs fire APs at mean rates that range from fewer than 1 to greater than 100 APs per second (s^{-1}). These so-called "spontaneous" APs are not generated cell-endogenously. Rather, both spontaneous and sound-evoked APs require the endocochlear potential, IHC depolarization, voltage-gated Ca^{2+} influx, and glutamate release from the IHC AZ onto its paired SGN bouton (Sewell, 1984; Glowatzki & Fuchs, 2002; Robertson & Paki, 2002).

5.1.5 Voltage-Gated Ca^{2+} Channels Controlling Exocytosis

Continuous, graded receptor potentials arise from mechanoelectrical and voltage-gated conductances (Corey & Hudspeth, 1979; Roberts et al., 1990). These changes in hair cell transmembrane potential modulate the temporal pattern of synaptic voltage-gated Ca^{2+} channel activity. Gating of Ca^{2+} channels modulates synaptic transmission by triggering exocytosis of glutamate from synaptic vesicles. In the cochlea, the receptor potential of each IHC is sampled over time by several SGNs, separately, based on the details of Ca^{2+} channel activity at each presynaptic AZ. Therefore the synaptic transfer function can differ among synapses stimulated by the same IHC receptor potential.

Hair cells are said to release neurotransmitter continuously because their synapses are never truly at rest. From IHC AZs, glutamate is released in an ongoing temporal sequence of discrete quanta. These packets of glutamate arrive onto the SGN bouton at rates that increase with the level of depolarization of the IHC receptor potential, which changes in response to sound. In IHCs, the voltage-gated Ca^{2+} channels controlling exocytosis are not prone to use-dependent inactivation. Thus, IHC depolarization produces an increase in Ca^{2+} channel activity at each ribbon synapse that is sustained for the duration of the depolarization. The opening of just one voltage-gated Ca^{2+} channel may be sufficient to trigger exocytosis of glutamate onto the SGN postsynaptic bouton (Sect. 5.3).

5.1.6 Abbreviations Used in This Chapter

AMPAR	α-Amino-3-hydroxy-5-methyl-4-isoxazolepropionic acid receptor
AP	Action potential
AZ	Active zone
BAPTA	1,2-*bis*(o-aminophenoxy)ethane-*N*,*N*,*N*′,*N*′-tetraacetic acid, "fast" Ca^{2+} chelator
$[Ca^{2+}]$	Ca^{2+} concentration
C_2	Ca^{2+}-binding protein domain
CaBP	Ca^{2+} binding protein
$Ca_V1.3$	Voltage-gated Ca^{2+} channel, L-type, pore-forming α-1D subunit
$Ca_Vß$	Auxiliary ß-subunit of voltage-gated Ca^{2+} channel
$Ca_Vα2δ$	Auxiliary α2δ-subunit of voltage-gated Ca^{2+} channel
CDI	Ca^{2+}-dependent inactivation
CtBP2	C-terminal binding protein 2
EGTA	Ethylene glycol-*bis*(2-aminoethylether)-*N*,*N*,*N*′,*N*′-tetraacetic acid, "slow" Ca^{2+} chelator
EPSC/P	Excitatory postsynaptic current/potential
ex vivo	Experiments in acutely explanted organs
GluA	Glutamate receptor subunit type, comprising AMPARs
HCN	Hyperpolarization-activated, cyclic nucleotide-gated nonspecificationic current (I_h)
IHC	Inner hair cell
K_V	Voltage-gated K^+ channel
m	Apparent Ca^{2+} cooperativity of exocytosis; from a power function fit to the relationship between exocytosis and Ca^{2+} influx
Na_V	Voltage-gated Na^+ channel
PSD	Postsynaptic density
px	Postnatal day *x*
RRP	Readily releasable pool of vesicles
SGN	Type I spiral ganglion neuron, also called auditory nerve fiber, cochlear nerve fiber, or auditory nerve single-unit

SNARE Soluble NSF attachment protein receptors, including SNAP, syntaxin, and synaptobrevin proteins
SR Spontaneous AP rate of a SGN (in the absence of sound)

5.2 Synaptogenesis of IHC and Type I Spiral Ganglion Neuron

5.2.1 Development from Pattern Generator to Sound Receiver

Before the onset of sensory function, IHCs drive patterned APs in the auditory nerve that seem to be required for normal wiring of the auditory brain (Walsh & McGee, 1987; Clause et al., 2014). These presensory APs in SGNs are driven by synaptic transmission, evoked by Ca^{2+} spikes in immature IHCs (Fig. 5.2a–c). Calcium spikes are regenerative potentials, similar to Na^{+} APs in neurons. Spike-driven exocytosis in immature IHCs (Kros et al., 1998; Beutner & Moser, 2001) is mediated predominantly by $Ca_V1.3$ Ca^{2+} channels (Brandt et al., 2003; Marcotti et al., 2003). Although mature IHCs do not spike, they use the same type of voltage-gated Ca^{2+} channels to mediate hearing.

By the onset of hearing, at approximately postnatal day 14 (p14) in mice and rats, reduction in number of $Ca_V1.3$ channels (Brandt et al., 2003) and upregulation of K^{+} channels disable regenerative Ca^{2+} spikes in IHCs. For example, the large-conductance Ca^{2+}- and voltage-activated K^{+} channels (BK channels) carry a hyperpolarizing conductance that ensures a nonspiking, graded response of the mature IHC transmembrane potential (Kros et al., 1998; Oliver et al., 2006). Another developmentally upregulated K^{+} channel, $K_V7.4$ ($KCNQ_4$,), defective in human deafness DFNA2 (Kubisch et al., 1999), is partially active when IHCs are at rest, and contributes to setting the IHC resting membrane potential (Oliver et al., 2003). Many aspects of IHC development depend on thyroid hormone signaling (Rüsch et al., 2001; Sendin et al., 2007).

Presensory spiking in IHCs generates bursts of APs in SGNs at p10 in vivo (Fig. 5.2c). These bursts are replaced by mature-looking AP trains in SGNs around p14 (Wong et al., 2013). Experiments in organ of Corti explants have investigated what underlies the temporal pattern of Ca^{2+} spikes in IHCs, but the mechanism is still under debate. Release of ATP onto IHCs from cells in the developmentally transient Kölliker's organ may be important for hair cell excitation (Tritsch et al., 2007; Tritsch & Bergles, 2010), although patterned activity proceeded in the presence of inhibitors of ionotropic purinoceptors (Sendin et al., 2014). Alternatively, patterned electrical activity may be intrinsic to the IHC but modulated by ATP release (Johnson et al., 2011).

There is general agreement that presensory activity is likely regulated by inhibition of IHCs via the efferent synapses of olivocochlear neurons. Inhibitory

cholinergic transmission could periodically interrupt the IHC depolarization resulting from resting mechanotransduction (Walsh & Romand, 1992; Glowatzki & Fuchs, 2000; Sendin et al., 2014), similar to efferent inhibition of mature outer hair cells (Géléoc & Holt, 2003). However, olivocochlear neurons have somas in the brain, and it is unclear how intrinsic activity in their axons is altered in the excised organ of Corti. Whatever the mechanism, dramatic changes in SGN AP trains between p10 and p14 (Fig. 5.2c–f) are concurrent with IHC synaptic maturation.

5.2.2 Anatomical and Physiological Synaptic Maturation

In mice, SGN fibers reach cells in the differentiating organ of Corti already at birth. The numbers of fibers and synapses in the organ of Corti appear to increase in number during the first postnatal week (Lenoir et al., 1980; Shnerson et al., 1981). Then, presynaptic ribbons and postsynaptic densities (PSDs) decrease in number (Huang et al., 2007, 2012). By p21, IHC–SGN synapses are predominantly mature (Sobkowicz et al., 1982; Grant et al., 2010). This section highlights some structural and functional aspects of synaptic maturation and discusses underlying molecular-anatomical mechanisms.

In the first postnatal week, the IHC Ca^{2+} current and exocytosis increase as they approach their peak sizes. Then, during the second postnatal week, they decline differently as the efficiency with which Ca^{2+} influx triggers exocytosis increases. The number of $Ca_V1.3$ channels decreases but the smaller Ca^{2+} current of mature IHCs causes comparably large amounts of exocytosis (Beutner & Moser, 2001; Brandt et al., 2005; Zampini et al., 2010). Immunofluorescence microscopy in fixed tissue (Fig. 5.3a–c) as well as Ca^{2+} imaging in live tissue revealed that overall $Ca_V1.3$ immunoreactivity declined while it accumulated synaptically and the Ca^{2+} influx increased specifically at the ribbon synapses (Wong et al., 2013, 2014). Thus, maturation involved reduction of extrasynaptic Ca^{2+} channels not directly coupled to synaptic vesicle exocytosis. Unlike immature IHCs, Ca^{2+} influx in mature IHCs is largely confined to AZs.

Individual IHC–SGN synapses at p6 displayed several small appositions of AZs and PSDs, only some of them occupied by a presynaptic ribbon. These groups of appositions encircled the perimeter of the bouton contact (Wong et al., 2014). Only after the onset of hearing was a single juxtaposed AZ–PSD complex found per SGN bouton (Fig. 5.3).

As AZs and PSDs decreased in number they increased in size, as shown via electron microscopy (Fig. 5.3e, f) and corroborated with confocal immunohistochemistry using antibodies against $Ca_V1.3$ Ca^{2+} channels, GluA2/3 glutamate receptors, and the ribbon protein CtBP2 (Fig. 5.3a–c; Wong et al., 2014). The ratio of ribbons to glutamate receptor puncta increased to nearly 1 by p20, indicating that ribbonless AZs disappeared and the 1:1 connection between ribbons and PSDs prevailed for each SGN.

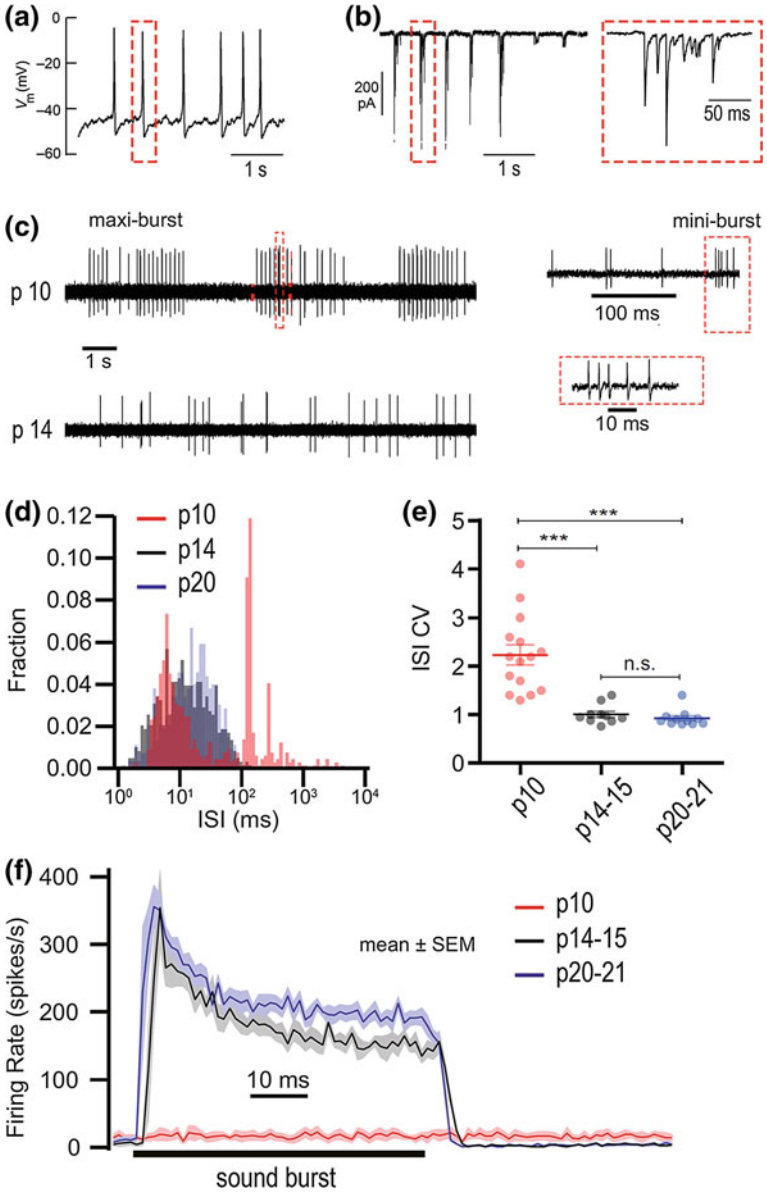
(a)
0
−20
−40
−60
V_m (mV)
1 s
(b)
200 pA
1 s
50 ms
(c)
maxi-burst
mini-burst
p 10
1 s
100 ms
10 ms
p 14
(d)
0.12
0.10
0.08
0.06
0.04
0.02
0.00
Fraction
p10
p14
p20
10^0
10^1
10^2
10^3
10^4
ISI (ms)
(e)
5
4
3
2
1
0
ISI CV
***
***
n.s.
p10
p14-15
p20-21
(f)
400
300
200
100
0
Firing Rate (spikes/s)
mean ± SEM
p10
p14-15
p20-21
10 ms
sound burst

◀ **Fig. 5.2** Functional maturation from pattern generator to stimulus transducer. **a** Patch-clamp recording of a semiperiodic sequence of Ca^{2+} spikes in a developing IHC. **b** *Left*, bursts of EPSCs in a patch-clamp recording of a developing SGN, due to presynaptic Ca^{2+} spikes in the IHC. *Right*, one burst is enlarged. Each Ca^{2+} spike and EPSC burst lasts for approximately 100 ms and consists of several events of exocytosis. **c** *Upper*, in vivo SGN spontaneous AP train at p10 showing semiperiodic discharge. Each SGN AP mini-burst (*red dashed boxes* in **c**) is evoked by a burst of EPSCs (*red dashed box* in **b**) triggered by a Ca^{2+} spike in the presynaptic IHC (*red dashed box* in **a**). The timing between each mini-burst in a maxi-burst (the interburst interval) corresponds to the interspike interval in the immature IHC **a**. The periods between maxi-bursts represent durations over which the IHC is not spiking. *Lower*, SGN spontaneous AP train at p14 is relatively irregularly timed. **d** Interspike interval histograms for SGN spontaneous AP trains at p10, p14, and p20. The distribution of intervals changes from bimodal to unimodal between p10 and p14, and then remains relatively unchanged by p20. **e** Interspike interval coefficients of variation (CV: variance/mean) for individual SGN recordings (*filled circles*) and their means (*horizontal bars*) are significantly less by p14 because of the absence of long intervals that made the bimodal distribution at p10 **d**. **f** Mean instantaneous AP rates for repetitions of 50 ms sound bursts (*horizontal bar*) at the three developmental stages. After the onset of hearing (after p14) the SGNs exhibit an onset response that adapts and approaches a steady-state spike rate of $\sim$200 s^{-1}. (Modified from Wong et al., 2013. Concurrent maturation of inner hair cell synaptic Ca^{2+} influx and auditory nerve spontaneous activity around hearing onset in mice. *Journal of Neuroscience*, 33 (26), 10661–10666)

Ribbons are synaptically anchored via the presynaptic protein bassoon (Khimich et al., 2005). In keeping with the notion that Ca^{2+} channels cluster underneath ribbons in the presynaptic density (schematized in Fig. 5.3d, g), bassoon and $Ca_V1.3$ immunofluorescence closely aligned in elongated stripes at p19 when measured with two-color stimulated emission depletion (STED) microscopy (Wong et al., 2014; Rutherford, 2015). In contrast, before the onset of hearing synaptic $Ca_V1.3$ channels formed only smaller spot-like clusters.

Two candidate mechanisms for this anatomical refinement are (1) merging—small AZs or PSDs of a synaptic contact coalesce via interactions of scaffold molecules possibly involving transsynaptic regulation and (2) pruning—small AZs and PSDs are selectively eliminated via protein degradation. Bassoon and the similar protein piccolo each inhibit ubiquitin ligase activity (Waites et al., 2013). Their greater abundance might protect the largest of the initially formed AZs.

These structural refinements are accompanied by developmental changes in synaptic function and changes in molecular composition. At p0, rodent IHCs show relatively little Ca^{2+} current or exocytosis. As mentioned previously in this section, this is followed by an increase during week 1, then a decrease in Ca^{2+} current but relatively little decrease in exocytosis during week 2. This increase in efficiency of exocytosis is at least partially due to the positioning of more $Ca_V1.3$ channels at AZs and fewer $Ca_V1.3$ channels away from AZs (Fig. 5.3a). Moreover, during the first postnatal week exocytosis seems to employ a different molecular program than later in development. For example, otoferlin, essential for exocytosis in mature IHCs, seems dispensable for presynaptic function at this early stage while the neuronal Ca^{2+} sensor of exocytosis synaptotagmin 2 is temporarily expressed (Beurg et al., 2010; Reisinger et al., 2011). In addition to the increase in efficiency

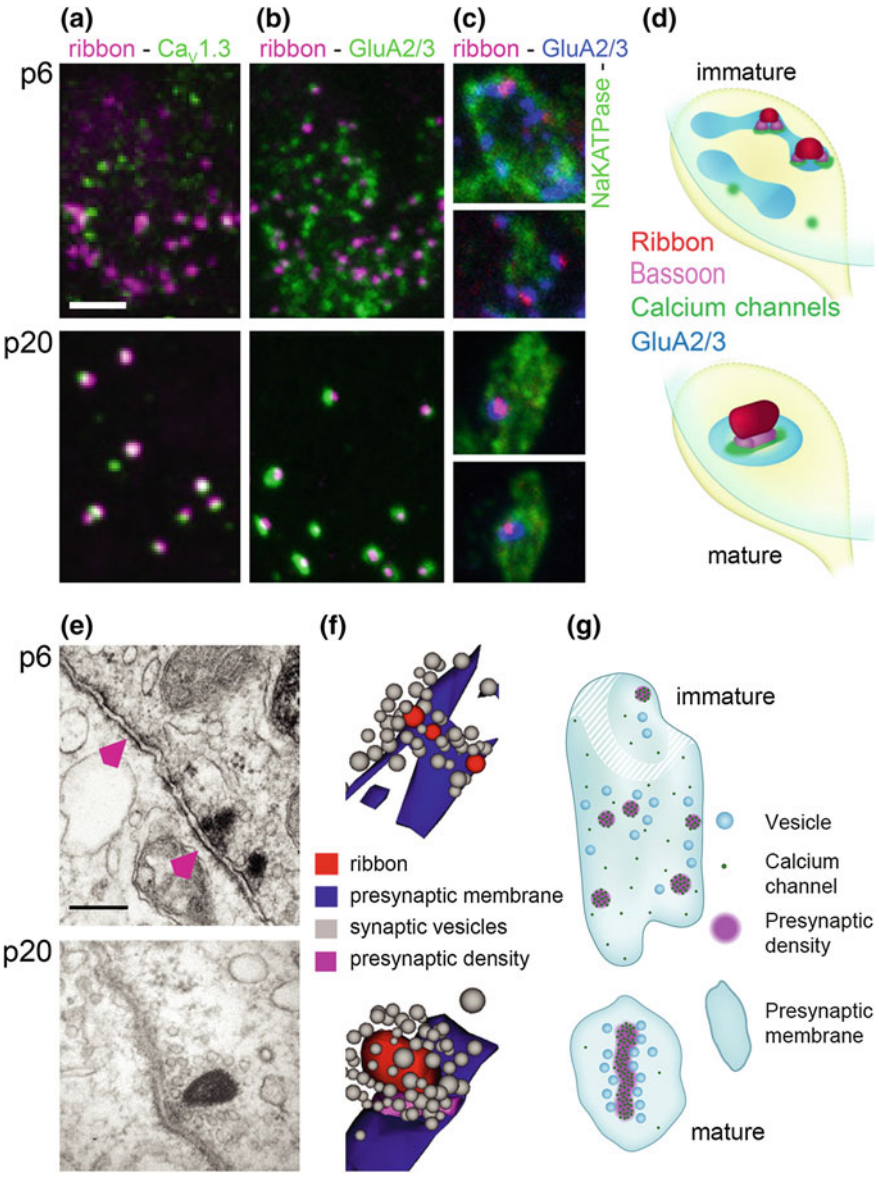
(a)
ribbon - $Ca_V1.3$
(b)
ribbon - GluA2/3
(c)
ribbon - GluA2/3
NaKATPase -
p6
p20
(d)
immature
Ribbon
Bassoon
Calcium channels
GluA2/3
mature
(e)
p6
p20
(f)
ribbon
presynaptic membrane
synaptic vesicles
presynaptic density
(g)
immature
Vesicle
Calcium channel
Presynaptic density
Presynaptic membrane
mature

◀ **Fig. 5.3** Structural maturation of IHC-SGN ribbon synapses. **a** Ribbons (anti-CtBP2, *magenta*) and voltage-gated Ca^{2+} channels (anti-$Ca_V1.3$, *green*) in one IHC at p6 (immature, *upper*) and one IHC at p20 (mature, *lower*). **b** Similar to **a** but with AMPA-type glutamate receptors on the green channel (anti-GluA2/3). Between p6 and p20, presynaptic voltage-gated Ca^{2+} channels and postsynaptic glutamate receptors become restricted to ribbons at IHC–SGN connections. **c** Ribbons (*magenta*), GluA2/3 (*blue*), and NaKATPase (*green*, labeling SGN boutons) demonstrate refinement of molecular anatomy within the synaptic regions defined by each bouton contact. **d** Schematic of changes in **a–c** illustrates the development of 1:1 connectivity between ribbons and SGNs between p6 and p20. **e** Electron micrographs of IHC–SGN synaptic contacts. At p6, some postsynaptic densities are juxtaposed to presynaptic ribbons while others are not (*magenta arrowheads*). By p20, almost all synapses have a single, larger ribbon. **f** Three-dimensional AZ reconstructions of a few small immature ribbons (p6, *upper*) and one large mature ribbon (p20, *lower*) anchored to the presynaptic membrane and surrounded by vesicles. **g** Schematic of IHC–SGN synapses shows a more ordered arrangement of voltage-gated Ca^{2+} channels and synaptic vesicles upon maturity. (Modified from Wong et al., 2014. Developmental refinement of hair cell synapses tightens the coupling of Ca^{2+} influx to exocytosis. *The EMBO Journal*, 33(3), 247–264; Copyright Wiley-VCH Verlag GmbH & Co. KGaA. Reproduced with permission)

of exocytosis, a change is also observed in the apparent Ca^{2+} dependence of exocytosis when manipulating the Ca^{2+} current by changing the number of open channels (Johnson et al., 2005; Wong et al., 2014).

Two mechanisms have been proposed to contribute to changes in the Ca^{2+} efficiency and apparent Ca^{2+} dependence of exocytosis in IHCs around the onset of hearing: (1) the intrinsic Ca^{2+} dependence of exocytosis changes due to a switch in synaptic protein type and/or (2) tightening of the spatial coupling between Ca^{2+} channels and vesicles at the AZ. A developmental upregulation of synaptotagmin IV has been proposed to underlie the increase in Ca^{2+} efficiency and the linearization of the apparent Ca^{2+} dependence of IHC exocytosis around the onset of hearing (Johnson et al., 2010), which might support hypothesis 1.

The intrinsic Ca^{2+} dependence of exocytosis in mouse IHCs was compared before and after the onset of hearing by measuring the Ca^{2+}-dependent rate constant of the fast component of exocytosis, elicited by step changes of $[Ca^{2+}]$ in response to intracellular Ca^{2+} uncaging (Wong et al., 2014). The intrinsic Ca^{2+} dependence was found to be similar, which does not support hypothesis 1. In contrast, when changing the Ca^{2+} current by manipulating the number of open channels, a developmental difference was found in the apparent Ca^{2+} dependence (or cooperativity) of exocytosis. The apparent Ca^{2+} cooperativity of exocytosis was supralinear before hearing onset but near linear in mature IHCs, suggesting a transition from Ca^{2+} *micro*-domain control of exocytosis before the onset of hearing to Ca^{2+} *nano*-domain control of exocytosis after the onset of hearing. Development of Ca^{2+} nanodomain control of exocytosis upon maturation implies tightening of the spatial coupling between Ca^{2+} influx and exocytosis, which supports hypothesis 2. Indeed, the topography of membrane-proximal vesicles, assumed to form the readily releasable pool, is more ordered around presynaptic densities after the onset of hearing (Fig. 5.3g). For more on the subjects of intrinsic and apparent Ca^{2+}

cooperativity as well as Ca^{2+} microdomain and nanodomain control of exocytosis, see Sect. 5.3.3.

5.3 Presynaptic Mechanisms Encoding Sound

5.3.1 Presynaptic Ca^{2+} Influx

Unlike typical L-type Ca^{2+} currents known in other systems to be activated by high-voltage (e.g., in cardiomyocytes of the heart), the L-type Ca^{2+} currents in hair cells of the inner ear activate at relatively hyperpolarized potentials, exhibit fast activation, and undergo slow and mild inactivation (Fuchs et al., 1990; Roberts et al., 1990; Spassova et al., 2001). In mouse cochlea, the pore-forming alpha subunit is $Ca_V1.3$ (Platzer et al., 2000; Brandt et al., 2003; Dou et al., 2004). Without Ca^{2+} influx through this channel, IHC synaptic exocytosis is abolished (Moser & Beutner, 2000; Brandt et al., 2003) and there is profound deafness in rodents and humans (Zhang et al., 1999; Platzer et al., 2000; Baig et al., 2011).

Hair cells are thusly similar to retinal photoreceptors and bipolar neurons, which also employ L-type Ca^{2+} channels, have synaptic ribbons, and transduce graded receptor potentials for controlling transmitter release (Barnes & Hille, 1989; Heidelberger & Matthews, 1992; Tachibana et al., 1993). They are different from conventional central nervous system (CNS) synapses that use N- and P/Q-type Ca^{2+} channels for transmitter release. The number of channels depends on species, developmental stage, and AZ number which varies by tonotopic location but, on average, the number of Ca^{2+} channels per mature mouse IHC is approximately 1700, with the majority being synaptic (Brandt et al., 2005; Frank et al., 2010; Wong et al., 2014). Evidence from various technical approaches agrees that each AZ of a mature auditory hair cell has on average approximately 100 Ca^{2+} channels in the frog (Roberts et al., 1990; Issa & Hudspeth, 1996; Rodriguez-Contreras & Yamoah, 2001), turtle (Tucker & Fettiplace, 1995), and mouse (Brandt et al., 2005; Zampini et al., 2013).

IHC $Ca_V1.3$ currents have little Ca^{2+}-dependent inactivation (CDI) and activate at relatively negative potentials (Koschak et al., 2001), likely due to the IHC-specific molecular composition of the $Ca_V1.3$ Ca^{2+} channel complex and specific intracellular modulators of its activity. $Ca_V\beta_2$ was identified to be the predominant ß-subunit of IHCs that co-regulates channel inactivation and enables sufficient numbers of Ca^{2+} channels to accumulate at the AZ (Neef et al., 2009). The $Ca_V\alpha2\delta$ subunit(s) involved in the IHC Ca^{2+} channel remain to be identified. Calmodulin, an obligate mediator of CDI (Lee et al., 2000), is expressed in IHCs, where it regulates CDI of $Ca_V1.3$ channels (Grant & Fuchs, 2008). However, calmodulin-mediated CDI of $Ca_V1.3$ channels is antagonized by Ca^{2+} binding proteins (CaBPs), several of which are expressed in IHCs (Yang et al., 2006; Cui

et al., 2007). In humans, mutation in the gene coding for CaBP2 results in hearing impairment DFNB93 (Schrauwen et al., 2012).

The list of putative regulators of the IHC $Ca_V1.3$ Ca^{2+} channel complex is steadily growing and includes bassoon, Rab3-interacting molecule (RIM), RIM-binding protein (Hibino et al., 2002), harmonin, and otoferlin. Of the two described mechanisms of interaction between RIM and Ca^{2+} channels, via RIM–PDZ binding to the proline-rich PDZ interacting motif in the C-terminus of $Ca_V\alpha$ or via RIM C-terminal C_2 domain binding to Ca_Vß, the $Ca_V1.3$ Ca^{2+} channel complex seems to employ only the C_2 domain-Ca_Vß binding (Gebhart et al., 2010; Kaeser et al., 2011). Harmonin, a scaffold protein mutated in Usher 1C syndrome (Verpy et al., 2000), is an important organizer of the mechanotransduction machinery in the hair bundle. Harmonin also interacts with $Ca_V1.3$ via binding of its second PDZ domain to the proline-rich PDZ interacting motif in the $Ca_V1.3$ C-terminus (Gregory et al., 2011). In this interaction harmonin imposes an inhibition on $Ca_V1.3$ gating that is relieved by depolarization, thereby contributing to voltage-dependent facilitation of $Ca_V1.3$. In addition, harmonin appears to facilitate ubiquitination and proteasomal degradation of $Ca_V1.3$, potentially co-regulating the abundance of Ca^{2+} channels at the presynaptic AZ (Gregory et al., 2011). Finally, proper number and morphology of $Ca_V1.3$ Ca^{2+} channel clustering have been attributed to the presynaptic scaffold protein bassoon and/or its associated supramolecular ribbon nanomachine (Frank et al., 2010; Jing et al., 2013). IHCs from mice lacking function of bassoon protein had fewer ribbons and less Ca^{2+} channel immunofluorescence at AZs (Fig. 5.4a). Reduction of Ca^{2+} channel immunoreactivity was greatest at the ribbonless AZs. Because the remaining ribbons were more loosely anchored to the AZ than wild-type ribbons (Fig. 5.4b, c), the extent to which functional deficits were due to lack of bassoon alone versus disruption of the entire ribbon complex is unclear.

Presynaptic Ca^{2+} influx has been imaged in living hair cells with confocal microscopy in excised inner ear endorgans. On strong depolarization, spatially confined Ca^{2+} signals rapidly rise and decay with two time constants (Issa & Hudspeth, 1996; Frank et al., 2009), dependent on cytosolic diffusion of free and buffered Ca^{2+} (Roberts, 1993). Among IHC AZs, a marked heterogeneity of Ca^{2+} signal amplitude and voltage of half-maximal activation was observed (Frank et al., 2009). This presynaptic heterogeneity may enable the IHC to decompose sound amongst SGNs having different sensitivities, to encode the entire audible range of sound pressures at any characteristic frequency. For more about synaptic heterogeneity, see Sect. 5.5.

5.3.2 *Presynaptic Transmitter Release*

The ensuing Ca^{2+} signal drives rapid exocytosis of the readily releasable pool (RRP) of synaptic vesicles at the AZ, which releases glutamate onto the postsynaptic SGN bouton (Sect. 5.4). The IHC AZ has a molecular composition and

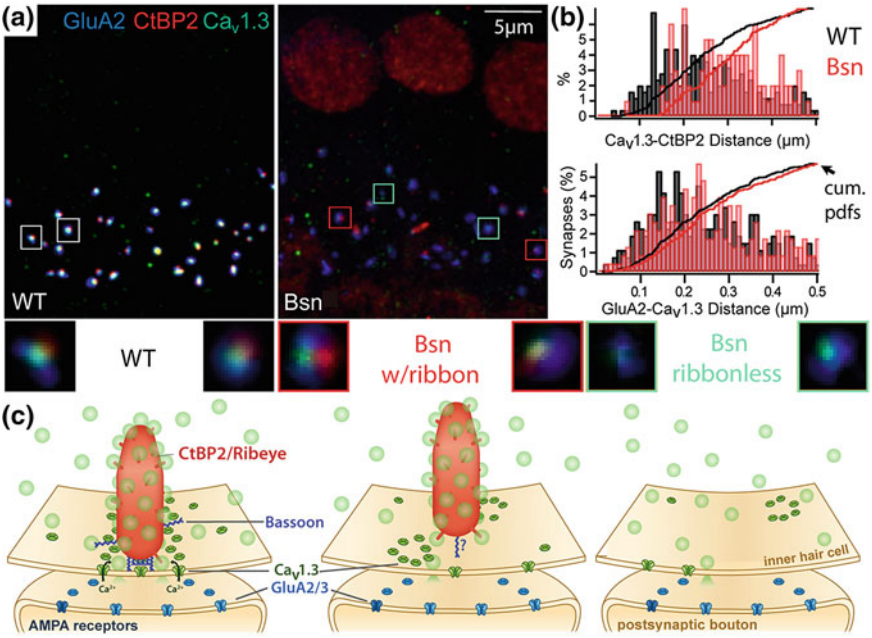

Fig. 5.4 Bassoon anchors the ribbon to the active zone, organizing Ca^{2+} channels and vesicles. **a** AMPA receptors (anti-GluA2, *blue*), ribbons (anti-CtBP2, *red*), and Ca^{2+} channels (anti- $Ca_V1.3$, *green*) in mature IHCs of wild-type mice (*left*, WT) or bassoon-deficient mice (*right*, Bsn). In Bsn IHCs, a minority of ribbons remained and all AZs appeared to have fewer Ca^{2+} channels. Small boxes are centered on individual AZs enlarged below for WT synapses (*white boxes, left*), ribbon-occupied Bsn synapses (*red boxes, center*), and ribbonless Bsn synapses (*aqua boxes, right*). **b** Analysis per AZ: without bassoon (*red*, Bsn) the distances between CtBP2 and $Ca_V1.3$ puncta (*upper*) are greater than in wild-type (*black*, WT). The distance between GluA2 and $Ca_V1.3$ puncta (*lower*) was relatively unaffected. *Vertical bars* are frequency histograms and lines are cumulative probability density functions (cum. pdfs). **c** Schematic of protein localizations at AZs of WT (*left*), ribbon-occupied Bsn (*middle*), and Bsn ribbonless IHCs (*right*). (Modified from Jing et al., 2013. Disruption of the presynaptic cytomatrix protein bassoon degrades ribbon anchorage, multiquantal release, and sound encoding at the hair cell afferent synapse. *Journal of Neuroscience*, 33(10), 4456–4467)

structure that enables temporally precise release at high rates over long periods of time, as required for normal hearing (Moser et al., 2006; Matthews & Fuchs, 2010; Rutherford & Pangršič, 2012). The synaptic ribbon tethers synaptic vesicles to its ellipsoid-like surface. Moreover, two rows of vesicles align with the presynaptic membrane density at the base of the ribbon (Frank et al., 2010), some tethered to the plasma membrane. Because of their number and their preferential loss during stimulation, these vesicles are often considered to be the ultrastructural substrate of a finite RRP measured physiologically (Moser & Beutner, 2000; Lenzi et al., 2002). The vesicles immediately surrounding and near ribbons are thought to refill the RRP. Vesicle density can differ between high- and low-frequency hair cells, which

may be an important tonotopic specialization (Schnee et al., 2005). After fusion with the plasma membrane, vesicles are regenerated via endocytosis in the perisynaptic space (Neef et al., 2014).

Sound-response properties of single auditory nerve units have been measured with extracellular electrophysiological recording of APs from the central axon of single SGNs in vivo (Kiang, 1965; Taberner & Liberman, 2005). The 1:1 connectivity between IHC AZ and SGN makes these recordings extremely valuable for understanding sound encoding at the IHC afferent synapse but also, more generally for neuroscience, because there is probably no other synaptic connection for which an in vivo readout of a single AZ exists. Computational models have used the acoustic signal as input and the APs of individual SGNs as measured output to describe cochlear filter properties mathematically (Weiss, 1966; Meddis, 2006).

To measure exocytosis of synaptic vesicles, the patch-clamp technique was applied to hair cells in inner ear explants (Parsons et al., 1994). Patch-clamp measurements of presynaptic plasma membrane capacitance allow one to monitor exocytosis and endocytosis because fusion and fission of synaptic vesicle membrane with plasma membrane cause increases and decreases, respectively, in surface area that are proportional to capacitance. Applied to the whole cell, measurements of capacitance changes report the summed activity of all synapses. On average, each AZ in a mouse IHC has RRP of about one dozen vesicles that undergoes exocytosis with a time constant of about 10 ms and is replenished with fast and slow time constants of about 140 ms and 3 s (Moser & Beutner, 2000). For single AZ measurements of exocytosis and synaptic transmission with the patch-clamp technique applied to SGN boutons, see Sect. 5.4.2.

Insights into the molecular composition of transmitter release have been provided along three main avenues of investigation: (1) candidate gene approaches driven by knowledge of conventional synapses (e.g., Safieddine & Wenthold, 1999; Nouvian et al., 2011), (2) genetics of human deafness (e.g., Yasunaga et al., 1999; Ruel et al., 2008), and (3) proteomics (Uthaiah & Hudspeth, 2010; Kantardzhieva et al., 2012; Duncker et al., 2013). The synaptic ribbon is composed primarily of the protein Ribeye (Schmitz et al., 2000), a splice variant of the transcriptional co-repressor CtBP2 that has lysophosphatidylacyl-transferase activity (Schwarz et al., 2011). The presence of ribeye at AZs seem to promote endocytic vesicle regeneration, vesicle tethering/docking/priming, and Ca^{2+}-channel clustering in hair cells (Frank et al., 2010; Sheets et al., 2011; Jing et al., 2013; Khimich et al., 2005).

Some components of the presynaptic AZ machinery seem not to be conserved between conventional neuronal synapses and ribbon-type synapses of IHCs, specifically the proteins that mediate Ca^{2+} sensing and lipid membrane fusion. Otoferlin, a multi-C_2-domain ferlin protein specifically expressed in inner ear hair cells is defective in human deafness DFNB9 (Yasunaga et al., 1999) and is currently the best candidate for a vesicular Ca^{2+} sensor. Exocytosis was nearly abolished in otoferlin-deficient IHCs despite the presence of synaptic vesicles at the AZ (Roux et al., 2006). A definitive conclusion on otoferlin as a Ca^{2+} sensor of fusion will require mutagenesis of Ca^{2+} binding sites, biochemical characterization of altered Ca^{2+} binding, and physiological assessment of the Ca^{2+} dependence of IHC

exocytosis with the mutant otoferlin. In addition to its putative role as Ca^{2+} sensor, otoferlin seems to facilitate vesicle replenishment (Pangršič et al., 2010).

The core membrane fusion machinery is thought to be conserved at all synapses. In neurons it consists of the soluble NSF attachment protein receptors (SNAREs) synaptobrevin 1 or 2, SNAP25, and syntaxin 1. However, experiments that used neurotoxins and genetic mutations to disable SNARE proteins indicated that IHC exocytosis may operate without neuronal SNARE proteins (Nouvian et al., 2011). Interestingly, otoferlin has been shown to interact with neuronal SNAREs (Roux et al., 2006; Ramakrishnan et al., 2009) but hair cells seem to lack SNARE regulators such as synaptotagmins (Beurg et al., 2010; Reisinger et al., 2011) and complexins (Strenzke et al., 2009; Uthaiah & Hudspeth, 2010). Investigations into the fusion machinery of IHCs are ongoing.

5.3.3 *Stimulus–Secretion Coupling*

There is an intimate functional relationship and perhaps even direct molecular binding between release-ready vesicles and Ca^{2+} channels in a proximity of 10–30 nm. From the perspective of the Ca^{2+}-sensing protein on a given release-ready synaptic vesicle, it seems that only one or very few $Ca_V1.3$ channels dominate the local $[Ca^{2+}]$ (Brandt et al., 2005; Goutman & Glowatzki, 2007; Graydon et al., 2011). In other words, Ca^{2+} control of exocytosis appears to operate in nanodomains. Alternatively, vesicle fusion at a given AZ may be controlled by a Ca^{2+} microdomain (Johnson et al., 2008, 2010; Heil & Neubauer, 2010), in which many Ca^{2+} channels contribute to the local $[Ca^{2+}]$ signal acting on individual vesicles.

To test the nanodomain versus microdomain hypotheses, the relative number of $Ca_V1.3$ channels contributing to exocytosis can be experimentally tested by studying the incremental dependence of RRP exocytosis on Ca^{2+} influx. The apparent Ca^{2+} cooperativity m is obtained by fitting a power function to the relationship between exocytosis and transmembrane Ca^{2+} charge (Q_{Ca}): exocytosis = $A(Q_{Ca})^m$, where A is the amplitude of the exocytic response and the exponent m is the apparent cooperativity. Different data points are obtained by manipulating the Ca^{2+} influx, either by changing the number of open channels or by changing the charge through each channel, while depolarizing the IHC for a brief duration to probe the RRP. If m is smaller when manipulating Ca^{2+} influx by changing the number of open Ca^{2+} channels than it is when changing the current through a given channel, then Ca^{2+} nanodomain control of exocytosis is suggested. If m is close to unity then the dependence of RRP exocytosis on Ca^{2+} influx is near linear. This implies little or no cooperativity of Ca^{2+} in its coupling to vesicle fusion and suggests nanodomain stimulus-secretion coupling. In the extreme interpretation of nanodomain, one vesicle undergoes exocytosis for each opening of a Ca^{2+} channel because a sufficient $[Ca^{2+}]$ is reached to saturate the sensor. Ca^{2+} from further channels would be insufficient. On the other hand, if comparable estimates of m are obtained for these two types of manipulation of Ca^{2+} influx (changing the number of open Ca^{2+}

channels versus changing the current through a given channel), then m should be similar to the intrinsic biochemical Ca^{2+} cooperativity of IHC exocytosis ($m = 4$; Beutner et al., 2001). This would suggest Ca^{2+} microdomain control (Augustine et al., 1991). In a Ca^{2+} microdomain control of exocytosis, many channels must open with overlapping effects before [Ca^{2+}] is high enough to evoke fusion.

Evidence for a nanodomain-like control as described in the preceding text was obtained using membrane capacitance measurements to assay the Ca^{2+} dependence of exocytosis in mature IHCs (Brandt et al., 2005; Wong et al., 2014). When changing the number of open Ca^{2+} channels, m was approximately 1.4. When changing the charge through each channel, m was above 3. Considering the number and open probability of Ca^{2+} channels, the distance to vesicles, the concentration and binding kinetics of Ca^{2+} buffers, and the Ca^{2+} binding properties of the Ca^{2+} sensor on the vesicle (Matveev et al., 2011), biophysical modeling was performed to evaluate the Ca^{2+} nanodomain hypothesis. The model predicted a vesicle-to-sensor coupling of less than 20 nm (Wong et al., 2014), in agreement with experiments that tested the differential effects on exocytosis of synthetic Ca^{2+} chelators having different binding rates (EGTA and BAPTA, Moser & Beutner, 2000; Goutman & Glowatzki, 2007). Therefore, the IHC–SGN synapse seems to operate in a nanodomain regime. In vestibular hair cells the Ca^{2+} influx per ribbon is significantly less; however, the nanodomain stimulus–secretion coupling may be even tighter than in mature IHCs (Vincent et al., 2014).

5.4 Synaptic Transmission and Action Potential Generation

5.4.1 Latency and Rate

After presynaptic Ca^{2+} influx evokes vesicular exocytosis of glutamate into the cleft, the transmitter binds to transmembrane proteins of the PSD: ionotropic α-amino-3-hydroxy-5-methyl-4-isoxazolepropionic acid (AMPA)-type glutamate receptors (AMPARs) on the SGN bouton (Glowatzki & Fuchs, 2002). This binding induces a conformational change in the receptor that initiates the final step in the process of synaptic transmission, influx of cations, which can be measured as an event of synaptic transmission called an excitatory postsynaptic current (EPSC). When the EPSC creates an excitatory postsynaptic potential (EPSP) in the SGN bouton that is large enough to depolarize the nearby AP generator to AP threshold, then an AP is initiated in the SGN. Note the electrophysiological concept of AP threshold (e.g., mV required to generate an AP) is distinct from the concept of SGN sound response threshold (decibels of sound pressure level (dB SPL) required to evoke a criterion AP rate; see Sect. 5.5).

SGN boutons have maximum dimensions of 1 or 2 µm where they contact IHCs (Merchan-Perez & Liberman, 1996). On this contact membrane is a ring-like postsynaptic array of AMPA receptors approximately 0.8 µm in outer diameter and

0.4 μm in inner diameter, on average (Meyer et al., 2009). If this array has an AMPA receptor density of 3000 μm^{-2} (freeze-fracture electron microscopy; Saito, 1990), then one bouton has approximately 1500 AMPA receptors, on average. By comparison, pyramidal spines in the hippocampus are estimated to have, at most, 10 times fewer AMPA receptors (Nusser et al., 1998). In the SGN, the large number of AMPA receptors allows for potent glutamatergic excitation of the electrically compact bouton and its connected cable, which has a diameter of only 0.1–0.8 μm (Liberman, 1980).

The IHC–SGN synaptic delay is approximately 0.8 ms of the 1.3 ms between sound onset and spike recorded in the auditory nerve (Palmer & Russell, 1986). Presynaptic voltage-gated Ca^{2+} channels are tightly coupled to synaptic vesicles at the AZ and activate with microsecond kinetics (Sects. 5.2 and 5.3). Still, synaptic transmission—including Ca^{2+} influx and binding to the exocytosis machinery, formation of the fusion pore, diffusion and binding of glutamate, and opening of the AMPA receptors—is the slowest of the processes between sound onset (i.e., stimulation at the eardrum) and SGN spike.

In mature cochlear IHCs, in the absence of an applied sound each AZ already releases neurotransmitter onto its postsynaptic bouton in a Ca^{2+}-dependent mechanism that depends on depolarization of the hair cell resting potential by the resting mechanoelectrical transduction current through the hair bundle (Sewell, 1984; Robertson & Paki, 2002; Farris et al., 2006). This background level of transmission is evident as a sequence of EPSPs that excite the SGN to fire a spontaneous pattern of APs at irregular intervals (Walsh et al., 1972; Siegel, 1992; Glowatzki & Fuchs, 2002). These APs in the absence of sound occur at a mean rate termed the spontaneous rate (SR); their relatively irregular timing is likely due to the stochastic nature of presynaptic release (reviewed by Kim et al., 2013).

To encode sound, mechanoelectrical transduction of an auditory stimulus depolarizes the IHC from its resting potential (Russell & Sellick, 1978). The depolarization-evoked activation of synaptic Ca^{2+} channels increases the rate of release events from the presynaptic IHC, thus raising the rates of EPSCs and APs in the SGN. At SGN sound response threshold (i.e., the SPL required to produce a just detectable increase in SGN AP rate; Galambos & Davis, 1944), the IHC is depolarized by less than 1 mV from its resting potential (Dallos, 1985). SGN sound response threshold is thought to be the underlying basis of perceptual hearing threshold.

One measure of response speed is the latency of the first AP after sound onset in electrophysiological recordings of SGNs in vivo. In response to sounds of moderate intensity and rapid onset (80 dB, submillisecond rise time), the first-spike latency in many SGNs is less than 2 ms (Buran et al., 2010). Response speed depends on stimulus strength: more intense stimuli evoke faster responses. For hearing, perceptual threshold is a function of temporal integration of sound pressure over time (Heil & Irvine, 1997; Heil & Neubauer, 2003). Evidence suggests that the integration happens in the ear at the IHC–SGN synapse and that loud sounds are heard before soft sounds because with increasing sound level the EPSC rate becomes greater, making first-spike latencies briefer (Heil & Neubauer, 2001). Biophysical

modeling showed how the initial EPSC rate depends on stimulus size and number of RRP vesicles to determine the latency and jitter of the first AP (Wittig & Parsons, 2008; Buran et al., 2010). IHCs from bassoon mutant mice had a smaller RRP and fewer Ca^{2+} channels at AZs (Frank et al., 2010). Their hearing phenotype was impaired coding of sound onset with delayed and jittered first-APs (Buran et al., 2010), leading to a drastic reduction of the spiral ganglion compound action potential (Khimich et al., 2005).

Paired IHC–SGN patch-clamp recordings showed most directly how initial EPSC latency and amplitude depend on stimulus properties. Increasing the level of the IHC depolarization reduced the latency and increased the amplitude of the onset EPSC in the SGN bouton (Goutman, 2012). The amplitude increase was likely due to EPSC superposition at stimulus onset rather than a change in the individual EPSC size (Sect. 5.4.3). In addition to this speeding of transmitter release latency by stronger IHC depolarization, the increased EPSC amplitude in the SGN will further reduce first-spike latency by accelerating AP generation (Rutherford et al., 2012). Thus, at the onset of a strong stimulus, expedited IHC exocytosis and faster SGN AP generation produce shorter first-spike latencies in the auditory nerve, explaining the faster perception of sound onset with increasing sound pressure level.

Gradations of the IHC receptor potential represent changes in sound pressure level but are limited in speed by the low-pass filter property of the IHC membrane resistance (R_m) and capacitance (C_m), which define the membrane time constant $\tau = R_m C_m$. For frequencies admitted by the RC time constant of the IHC membrane (generally, below a few kilohertz) periodic stimuli evoke periodic APs in SGNs. These APs occur at preferred times within the cycle of the periodic stimulus, in a phenomenon known as phase-locking (Galambos & Davis, 1944) that underlies localization of sounds in the horizontal plane (Knudsen & Konishi, 1979). The brain calculates the angle of the horizontal vector to the source of low-frequency sound by comparing the arrival times of APs between the two ears. The accuracy and reproducibility of encoding this interaural time difference in the ear and its transmission to the brain depends on the precision of IHC–SGN transmission and AP generation.

When the level of a pure tone is increased, the preferred phase of phase-locked spikes remains relatively unchanged (Rose et al., 1967; reviewed by Fuchs, 2005). A plausible biophysical explanation is offered by the hypothesis of a Ca^{2+} nanodomain control of exocytosis (Sect. 5.3). If exocytosis is evoked by a nanometer-spaced Ca^{2+} channel, then a high-micromolar $[Ca^{2+}]$ directly around the vesicle could make Ca^{2+} binding to the sensor occur at saturated rate. In this case, the speed of exocytosis would be limited by vesicle fusion with the plasma membrane once the nearby channel has opened, no matter how many other channels opened. Stimulus intensity would then primarily affect the number of activated channels, while having relatively little effect on kinetics of exocytosis and SGN response, given an adequate RRP (Moser et al., 2006). By making interaural time difference relatively insensitive to stimulus level, the brain could be provided with binaural cues that enable calculation of sound source location regardless of intensity.

Paired recordings from IHC–SGN synapses showed how multiple presynaptic mechanisms may combine to produce consistent release latencies across stimulus

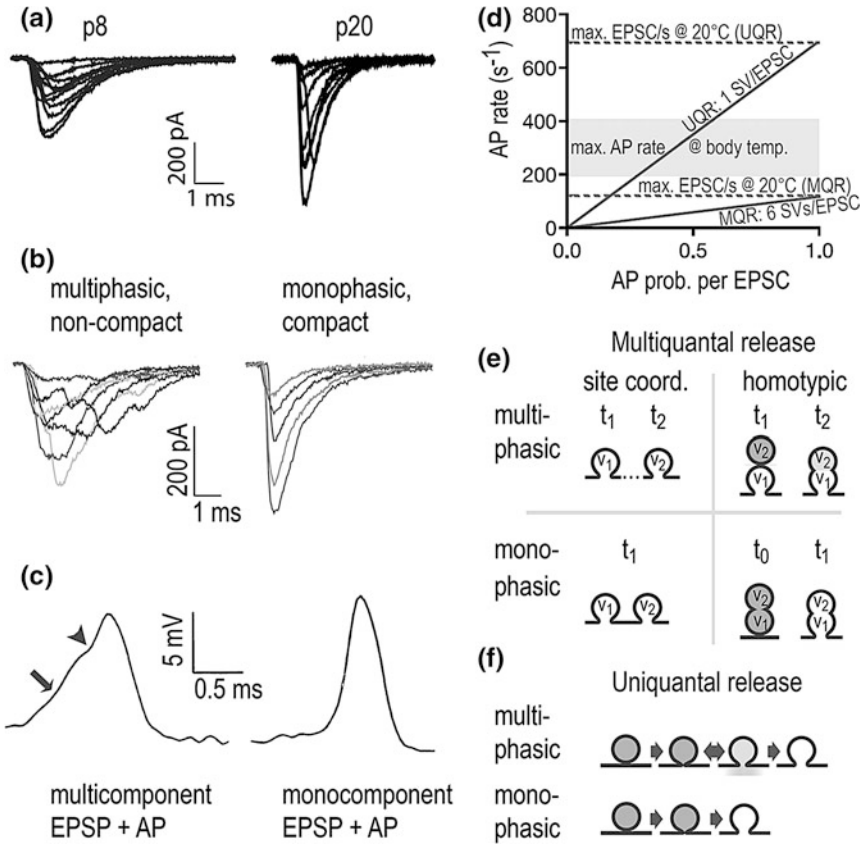

levels in response to the ongoing part of a periodic stimulus. The latency of synaptic transmission depended on the level of IHC depolarization. At the same time, it depended on stimulus history effects on presynaptic [Ca^{2+}] and the availability of release-ready vesicles (Goutman & Glowatzki, 2011 see also in the frog papilla: Cho et al., 2011; Li et al., 2014). A balance between Ca^{2+}-dependent presynaptic facilitation and vesicle supply-dependent presynaptic depression may underlie the near phase constancy of release as an ongoing periodic stimulus to the IHC is changed in intensity (Goutman, 2012).

5.4.2 Quantal Characteristics of Synaptic Transmission

It is believed that when transmission from an AZ is uniquantal, independent exocytosis of individual neurotransmitter-filled vesicles prevails. In contrast, in vivo intracellular recordings of SGN subthreshold potentials suggested that release of

◀ **Fig. 5.5** Synaptic vesicle exocytosis and postsynaptic response. **a** Between p8 and p20, monophasic EPSCs become larger and faster, as shown with patch-clamp intracellular recordings from SGN boutons. **b** Some EPSCs are temporally noncompact or multiphasic (*left*), but most are temporally compact or monophasic (*right*). **c** In vivo recordings of EPSPs demonstrate multiphasic (*left*) and monophasic (*right*) events of synaptic transmission preceding spontaneous APs. At *left*, the arrow points between two phases of the EPSP; *arrowhead* points to the onset of AP discharge. **d** *Diagonal lines* AP rate versus probability per EPSC under conditions of uniquantal release (UQR: one synaptic vesicle per EPSC) or multiquantal release (MQR: six synaptic vesicles per EPSC), assuming a maximum vesicle replenishment rate of 700 s^{-1}, as measured ex vivo at room temperature. The maximum EPSC rates for UQR (700 s^{-1}) and MQR (117 s^{-1}) are indicated by *dashed horizontal lines*. The *gray shaded area* indicates maximum sustained AP rates for SGNs in vivo at body temperature. **e** Schematic representation of two prominent hypotheses of synchronized multiquantal release: release site temporal coordination by a common Ca^{2+} nanodomain (*left*) and homotypic vesicle-to-vesicle fusion preceding compound exocytosis (*right*). Each mechanism could produce multiphasic (*upper*) or monophasic waveforms (*lower*). **f** The hypothesis of UQR with a dynamic fusion pore proposes that multiphasic (*upper*) and monophasic EPSCs (*lower*) result from flickering fusion and full fusion pore events, respectively. (**a** adapted from Grant et al. 2010. Two modes of release shape the postsynaptic response at the inner hair cell ribbon synapse. *The Journal of Neuroscience*, 30(12), 4210–4220. **b**, **d**, and **f** modified from Chapochnikov et al. 2014. Uniquantal release through a dynamic fusion pore is a candidate mechanism of hair cell exocytosis. *Neuron*, 83(6), 1389–1403. **c** adapted from Siegel 1992. Spontaneous synaptic potentials from afferent terminals in the guinea pig cochlea. *Hearing Research*, 59(1), 85–92)

multiple vesicles is synchronized even for generation of spontaneous APs (Siegel, 1992). Some EPSPs were brief while others were temporally dispersed, suggesting somewhat less synchronized release of several vesicles (Fig. 5.5c).

Pioneering intracellular patch-clamp recordings from SGN postsynaptic boutons of pre-hearing rats revealed enormous variability in EPSC amplitudes and waveforms (Glowatzki & Fuchs, 2002). Most EPSCs were waveforms that resembled alpha functions, with a fast and singular peak (i.e., monophasic) followed by a slower exponential decay. Although their peak amplitudes ranged from less than 30 pA to greater than 800 pA, monophasic EPSCs had similar kinetics. Some EPSCs had multiple peaks (multiphasic EPSCs). Monophasic EPSCs are temporally compact and multiphasic EPSCs are temporally dispersed (Fig. 5.5b). Although no precise mechanism is understood, monophasic and multiphasic EPSCs have been interpreted, respectively, as the postsynaptic responses to highly synchronized and poorly synchronized presynaptic release of multiple vesicles from a single AZ. Thus, IHC–SGN synaptic transmission seems more complex than what is expected under assumptions of uniquantal release. EPSC peak-amplitude distributions deviated from Gaussian, having high variance and positive skew, and means far greater than modes (means of 130–190 pA vs. modes of ∼36 pA). If the modal release event of approximately 30 pA represents release of one synaptic vesicle, then an EPSC of mean amplitude has a quantal content of four to six synaptic vesicles and the largest EPSCs have a content of approximately 20 vesicles (Glowatzki & Fuchs, 2002, their Fig. 4).

During maturation from p8 to p20, multiphasic EPSCs became even less frequent whereas monophasic EPSCs became larger and faster (Fig. 5.5a). The distribution of peak amplitudes became near Gaussian and the modal peak moved to approximately 375 pA as larger EPSCs became more frequent. Monophasic rise and decay times decreased from 0.6 to 0.3 ms and from 1.5 to 0.5 ms, respectively (Grant et al., 2010). The observation that the largest monophasic EPSCs can be as fast as the smallest monophasic EPSCs suggested that the range of EPSC peak amplitudes resulted from an extremely synchronized multiquantal multivesicular mechanism (Glowatzki & Fuchs, 2002, their Fig. 2; Keen & Hudspeth, 2006, their Fig. 2; Li et al., 2009, their Fig. 1).

Potential mechanisms of multiquantal release are schematized in Fig. 5.5e. One mechanism is pre-fusion of a variable number of vesicles followed by a single exocytic event (compound exocytosis; Fig. 5.5e, lower right: monophasic waveform at t_1 arising from homotypic multivesicular pre-fusion at t_0). Another possible mechanism is synchronous exocytosis of a variable number of single quanta (release-site coordination, Fig. 5.5e, lower left: monophasic event arising from simultaneous multivesicular release from multiple release sites at t_1), coordinated by, for example, a common Ca^{2+} signal (Graydon et al., 2011). Multiphasic EPSCs could represent the temporal overlap of nearly synchronous but staggered events of exocytosis, either through release site coordination or homotypic "piggy-back" fusion (Fig. 5.5e, upper left and right). These multivesicular mechanisms assume that exocytosis releases the full neurotransmitter content of each vesicle, such that transmission scales with the number of vesicles.

Assuming the mean EPSC quantal content to be 1 (i.e., uniquantal) or 6 (i.e., multiquantal) predicts quite different estimates of the numbers of vesicles required to support experimentally observed maximum sustained AP rates in SGNs in vivo, generally 200–400 s^{-1}. Given the rate of sustained IHC exocytosis from membrane capacitance measurements at room temperature, the maximal vesicle supply rate per AZ is estimated to be about 700 s^{-1} (Pangrsic et al., 2010). If each EPSC generates one AP and contains six vesicles on average, then an ongoing AP rate of 300 s^{-1} would require at least 1800 vesicles s^{-1} per AZ at body temperature. If each EPSC is univesicular, then higher AP rates are achievable with fewer vesicles (Fig. 5.5d), making release from a uniquantal vesicle seem more realistic. However, at body temperature, exocytosis from mature intact IHCs in response to sound is expected to exceed the maximal vesicle turnover rate per AZ of 700 s^{-1} estimated from patch-clamp electrophysiology at room temperature. This would increase the predicted AP rates in both the uniquantal and multiquantal scenarios.

As an alternative to multivesicular release, a uniquantal hypothesis is considered (Fig. 5.5f). Computational modeling of data on AMPA receptor number and ring-like morphology on SGN boutons suggested that EPSCs of maximum size can be evoked by the glutamate content of a single vesicle regardless of the precise location of the fusion event (Chapochnikov et al., 2014). This study suggested that short openings and flickering of the exocytic fusion pore could create multiphasic EPSCs and variably sized monophasic EPSCs from single vesicles. Additional variability between EPSCs arising from exocytosis of single vesicles could arise

from differences in vesicle volume (doubling the sphere diameter multiplies the volume by eight) or differences in neurotransmitter concentration (Wu et al., 2007). Experiments that combine electrophysiology and imaging may be required to elucidate the precise exocytosis mechanisms and, if they coexist, their relative contributions at hair cell ribbon synapses in different endorgans, species, and developmental stages.

How is AP generation in SGNs affected by EPSC variability? For the SR, the great majority of EPSPs successfully triggered an AP in vivo (~12 % failure rate, Siegel, 1992). Similarly, in the explanted organ of Corti, bouton recordings from relatively mature rats (p19) showed that the rates and interval distributions for EPSCs and APs were nearly identical (Rutherford et al., 2012). The nearly 1-to-1 conversion of EPSPs into APs for spontaneous AP rates, which are relatively low, indicated that in the absence of neural refractoriness only the smallest release events failed to trigger an AP in the SGNs tested. The situation may be different at higher rates, or in auditory endorgans of the turtle and frog, in which multiple hair cell AZs provide convergent input to each afferent neuron (Schnee et al., 2013; Li et al., 2014).

For the SR, it may seem wasteful that typical EPSCs (~300 pA) should so exceed the EPSC size required to reach AP voltage threshold. Indeed, when currents were injected into boutons through patch-pipettes, EPSC-like waveforms with amplitudes of less than 50–100 pA were already sufficient to depolarize the SGNs tested to spike threshold. However, the large EPSCs are likely required to achieve high AP rates in the presence of postsynaptic refractoriness. Further, large EPSCs improve the speed and precision of AP generation. Although small EPSCs triggered APs, increasing their size to the mean EPSC amplitude dramatically reduced latency and jitter. Spike-onset latencies improved from 1.5 to 0.5 ms when increasing the EPSC from 100 to 300 pA at room temperature (Rutherford et al., 2012).

5.4.3 *Short-Term Synaptic Depression Contributes to Spike Rate Adaptation*

The temporal pattern of sound-evoked APs depends on adaptation to stimulus history. Early experiments in the auditory nerve of cats demonstrated a progressive diminution in size of the population response during continued stimulation, which was not accompanied by any reduction in the gross cochlear potential (Derbyshire & Davis, 1935). This suggested that the IHC receptor potential was relatively nonadapting, and that sensorineural adaptation took place at the IHC–SGN synapse.

For example, fast AP rate adaption in the auditory nerve is an exponential decrement in AP rate following the initial peak at the onset of a sustained sound (Kiang, 1965). For tone bursts, this fast adaptation has two time constants of about 0.5 and 10 ms (Westerman & Smith, 1984). A similar reduction was not seen in the hair cell receptor potential or Ca^{2+} current (Russell & Sellick, 1978; Hudspeth & Lewis, 1988). Thus, fast adaptation is thought to arise from mechanisms

downstream from the Ca^{2+} current, like exhaustion of the RRP of synaptic vesicles (Furukawa & Matsura, 1978; Furukawa et al., 1982). Depletion of the RRP was indeed demonstrated by membrane capacitance measurements in hair cells and was shown to have similar kinetics as fast spike-rate adaptation in the same species (Moser & Beutner, 2000; Spassova et al., 2004; Buran et al., 2010). Figure 5.6b demonstrates the sustained IHC Ca^{2+} current for the duration of the stimulus. Exhaustion of the RRP at single AZs was observed directly with SGN recordings of EPSC trains during sustained IHC Ca^{2+} current (Fig. 5.6c, d; Goutman & Glowatzki, 2007).

Indeed, AP-rate decrement during a brief stimulus as well as AP-rate recovery between stimuli occur with time courses that mirror depletion and recovery, respectively, of the RRP. In recordings from IHC–SGN pairs in the organ of Corti explant (Fig. 5.6a), the recovery time constant of 37 ms for postsynaptic current amplitude in paired-pulse experiments ex vivo (Goutman, 2012) was similar to the time for half-recovery of the SGN AP rate in forward masking experiments in vivo (23 ms; Frank et al., 2010). Comparably fast paired-pulse recovery was measured in frog auditory hair cells at native temperature (Cho et al., 2011). Taken together, presynaptic mechanisms in the IHC seem to directly influence spike rate adaptation in SGNs.

The contributions of postsynaptic (i.e., SGN-intrinsic) mechanisms to SGN AP rate adaptation are less clear. However, fast adaptation is thought to be a mixture of both presynaptic depression and SGN refractoriness (Buran et al., 2010; Frank et al., 2010). Another form of response adaptation observed at the level of single SGNs in the auditory nerve is an adjustment of dynamic range—the range of sound pressure levels over which the SGN AP rate changes form minimum to maximum. Dynamic range adaptation depends on the mean level of sound in a continuously varying, dynamic stimulus (Wen et al., 2009). Future studies should address its underlying mechanisms.

5.4.4 Action Potential Generation

The distal-most segment of the SGN peripheral process, within the organ of Corti (i.e., within the inner spiral plexus, Fig. 5.1b), is sometimes called a dendrite. It has a compact morphology that supports potent synaptic transmission and robust AP generation. Patch-clamp recordings from SGN boutons of the rat showed high input resistance ($R_m \sim 0.5$–$3\ G\Omega$) and small input capacitance ($C_m \leq \sim 1$ pF; Glowatzki & Fuchs, 2002; Rutherford et al., 2012). A short distance away from the bouton ($\sim$20–40 µm) the SGN exits the organ of Corti, enters the spiral lamina, and gains myelin. There lies a heminode shown to contain voltage-gated Na^+ and K^+ channels ($Na_V1.6$ and $K_V1.2$; Lacas-Gervais et al., 2004; Hossain et al., 2005). The compact morphology and the voltage-gated conductances at the nearby heminode make the SGN very responsive to injected current.

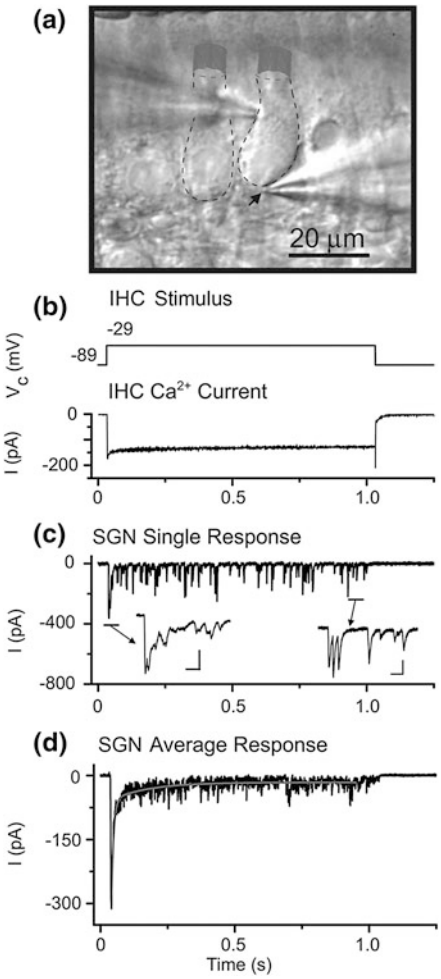

Fig. 5.6 Paired pre- and post-synaptic recordings demonstrate sustained presynaptic Ca^{2+} influx and depletion of the synaptic vesicle pool during prolonged IHC depolarization. **a** Photograph of a paired IHC–SGN electrophysiological recording in rat organ of Corti excised just before hearing onset. Two IHCs are outlined. The pipette on *left* records from an IHC while the pipette on *right* records from a SGN postsynaptic bouton (*arrow*). **b** The IHC is depolarized (*upper*) and the presynaptic voltage-gated Ca^{2+} current is activated and sustained (*lower*). **c** Example of the response recorded in the postsynaptic bouton. Each downward deflection is an individual EPSC; they superimpose somewhat at stimulus onset before the EPSC rate adapts. **d** Average of several responses from the same SGN illustrates depression of transmission due primarily to exhaustion of the presynaptic supply of releasable vesicles. (Adapted from Goutman and Glowatzki. Time course and calcium dependence of transmitter release at a single ribbon synapse. *Proceedings of the National Academy of Sciences of the USA*, 104(41), 16341–16346; Copyright (2007) National Academy of Sciences, USA)

In organ of Corti explants from mature rats (p19) SGN AP discharge was typically rapidly adapting, or phasic. When SGN boutons were depolarized with sustained current injection they fired only a single AP, at stimulus onset (Rutherford et al., 2012). Thus, high AP rates seem to require rapid repolarization of the SGN in between events of exocytosis, which may be aided by dendritic HCN channels (Yi et al., 2010). The molecular anatomy of primary afferent neurons in the inner ear is only beginning to be understood (Lysakowski et al., 2011). The phasic property is possibly due to SGN Na^+ channel inactivation (Santos-Sacchi, 1993). Curiously, the principal Na^+ channel isoform located at axon initial segments and nodes of Ranvier at neuronal synapses in the brain, $Na_V1.6$, is relatively resistant to inactivation and seems to promote repetitive firing (Raman et al., 1997). Other factors such as K^+ currents likely influence this phasic onset-response property in SGNs. This phasic property of SGN AP generation might prevent multiple APs during longer EPSCs, and thereby enhance the locking of AP times to the onsets of neurotransmitter release events (Rutherford et al., 2012).

5.5 Synaptic Heterogeneity and the Diversity of SGN Response Properties

5.5.1 Range Fractionation Through Synaptic Heterogeneity

Active amplification of cochlear vibrations at low sound levels and compression at high sound levels allows the entire 120 dB perceptual range of hearing to be encoded in the receptor potential of IHCs (Russell & Sellick, 1978). In contrast, individual SGNs have a smaller dynamic range: They change their AP rates from minimum to maximum over a more limited range of 10–40 dB of sound pressure level in cat, guinea pig, and gerbil (Sachs et al., 1989; Winter et al., 1990; Ohlemiller et al., 1991). In the mouse, most SGNs have dynamic ranges of less than 15 dB (Taberner & Liberman, 2005). Thus, the range of stimulus levels over which AP- rate changes in an individual SGN is much smaller than either the range over which loudness judgments can be made psychophysically or the range over which microphonic potentials measured at the round window increase in amplitude (Stevens & Davis, 1938/1983; Wever & Lawrence, 1954). One key hypothesis of wide dynamic range encoding is that information from one IHC receptor potential is somehow decomposed into the AP trains of multiple SGNs, each having different dynamic ranges: the hypothesis of range fractionation. A single mouse IHC has 7–20 presynaptic AZs and is innervated by 7–20 unbranched SGNs (Meyer et al., 2009), each of which encodes a fraction of the audible sound pressure range (Zagaeski et al., 1994).

To describe the diversity of response properties among single auditory nerve fibers recorded in vivo, SGNs can be categorized in terms of their SR and sensitivities to sound. These properties are interrelated and thought to arise from

underlying mechanisms that establish and maintain the firing behavior of a given SGN. In silence IHC AZs release glutamate at relatively low rates, evoking SRs that differ among SGNs from less than 1 to greater than 100 APs s^{-1}. Neurons with high SR are more sensitive to sound (i.e., lower threshold) than those with medium or low SR (Kiang, 1965; Liberman, 1978). SGNs of all characteristic frequencies exhibit this diversity. Therefore, SGNs with the same frequency tuning but different SRs and sound sensitivities are thought to emanate from neighboring if not the same IHC in the organ of Corti (Merchan-Perez & Liberman, 1996; Winter et al., 1990). The determinants of this afferent diversity are, however, unknown.

Downstream from cochlear mechanics and mechanoelectrical transduction, the specific sound-response properties of a given SGN depend on the details of the presynaptic AZ and the input–output function of the SGN itself. Thus, IHCs and SGNs may form diverse synaptic connections for SGNs to collectively encode the entire audible range. Differential sound encoding among SGNs may be regulated by afferent connections having different pre- and postsynaptic properties (Frank et al., 2009; Grant et al., 2010; Liberman et al., 2011) and by adjacent efferent synapses having different properties (Ruel et al., 2001). However, the ways in which SGNs and IHCs regulate synaptic heterogeneity are not clear.

5.5.2 *Presynaptic Heterogeneity*

The ribbon-type AZs of hair cells are large relative to AZs of conventional CNS synapses. Each IHC–SGN synapse is comprised of an AZ having several release-ready vesicles (i.e., the RRP) that can fuse with the plasma membrane in a few milliseconds after stimulation (Moser & Beutner, 2000). Neurotransmitter is released in response to graded depolarization, activating graded fractions of the population of voltage-gated Ca^{2+} channels at each AZ. The presence of numerous tethered synaptic vesicles and voltage-gated Ca^{2+} channels per IHC AZ plus evidence that relatively few of those Ca^{2+} channels regulate the exocytosis of individual vesicles (Sects. 5.3 and 5.4) contributed to the emerging view that individual IHC AZs are composed of multiple vesicular release sites (Nouvian et al., 2006).

Numerous release sites per IHC AZ is a property that seems essential for normal encoding of sound (Wittig & Parsons, 2008; Buran et al., 2010). The number of release sites likely scales with AZ size, which seems to differ among the AZs of a given IHC (Merchan-Perez & Liberman, 1996; Meyer et al., 2009). Understanding the differences in size among AZs in the IHC is a topic of current investigation. Synaptic ribbon size is a proxy for AZ size in hair cells. In the basilar papilla of the chick, the amplitude of the depolarization-evoked whole-cell Ca^{2+} current correlated positively with the whole-cell sum of ribbon cross sections (Martinez-Dunst et al., 1997). A systematic, tonotopic gradient was observed in which high-frequency basal hair cells had larger Ca^{2+} currents and larger AZ areas than hair cells in the low-frequency apex, suggesting that Ca^{2+} channel number and release site area are causally related.

In live Ca^{2+} imaging experiments, depolarization-evoked presynaptic Ca^{2+} signals around ribbons are termed Ca^{2+} microdomains (Fig. 5.7a). Ca^{2+} microdomain amplitudes are highly heterogeneous and positively correlated with the fluorescence intensity of ribbon-binding peptide (Fig. 5.7b), suggesting that larger Ca^{2+} microdomains arise from bigger AZs that contained more Ca^{2+} channels (Frank et al., 2009, 2010). The variance of Ca^{2+}-microdomain peak amplitudes in live tissue was larger than the variance of $Ca_V1.3$-immunofluorescence peak amplitudes in fixed tissue, suggesting that differences in channel regulation as well as channel number might contribute to synaptic heterogeneity among AZs. Indeed, the Ca^{2+} microdomain voltage dependence varies among the AZs within a given IHC. Ca^{2+}-microdomain variance exceeds that of the voltage dependence of whole-cell current activation between cells (Fig. 5.7c). This finding may reflect variation in composition among the supramolecular $Ca_V1.3$ channel complexes at each AZ. Each IHC decomposes auditory information into functionally diverse SGNs by divergence of its receptor potential through AZs that vary in synaptic strength.

Presynaptic Ca^{2+} influx is well known as a positive indicator of synaptic strength. In postnatal development of the mouse cochlea, IHC AZs with large-amplitude Ca^{2+} microdomains emerge around the onset of hearing, as do SGNs of high SR (Wong et al., 2013). In mature mice lacking function of bassoon protein, synaptic $Ca_V1.3$ channels are fewer in number. Ca^{2+} microdomains are smaller because there is less Ca^{2+} influx at AZs compared with wild-type (Fig. 5.7d, e; Bsn vs. WT). As a result there is less exocytosis from the IHC and abnormal encoding of sound in the auditory nerve (Khimich et al., 2005). SGNs in mice lacking bassoon have lower SRs and smaller dynamic ranges (Fig. 5.7f).

Like Ca^{2+} microdomains, presynaptic ribbons are heterogeneous in size. Larger ribbons and higher amplitude Ca^{2+} microdomains were observed more frequently on the modiolar-facing sides of IHCs (Meyer et al., 2009). If $Ca_V1.3$ expression, AZ size, and number of release sites are causally related, then modiolar-facing IHC AZs are expected to have stronger presynaptic function. However, cat SGNs with high SR and low threshold (i.e., high sensitivity to sound) were found more frequently on the pillar faces of IHCs, where ribbons are smaller (Merchan-Perez & Liberman, 1996). Thus, the relationships between AZ size, synaptic strength, and firing properties of the postsynaptic SGN are not clear. Moreover, this may constitute a conundrum. If $Ca_V1.3$ channel number scales with ribbon size and release site area, then how might larger ribbons with a larger RRP provide the synaptic input to SGNs that have lower SRs and lower sensitivities to sound?

Additional clues regarding the loci of heterogeneity contributing to SGN response diversity come from studies of facilitation, depression, and recovery in response to sounds in vivo and in response to direct IHC depolarization in organ of Corti explants. In response to pairs of clicks, the AP rates of low-SR SGNs facilitated while those of high-SR SGNs did not (Siegel & Relkin, 1987). Moreover, low-SR SGNs recovered from depression more slowly (Relkin & Doucet, 1991). Facilitation and depression are best understood as Ca^{2+}-dependent presynaptic mechanisms that depend on the probability of release and the availability of synaptic vesicles. At IHC synapses, facilitation and depression are at least partly

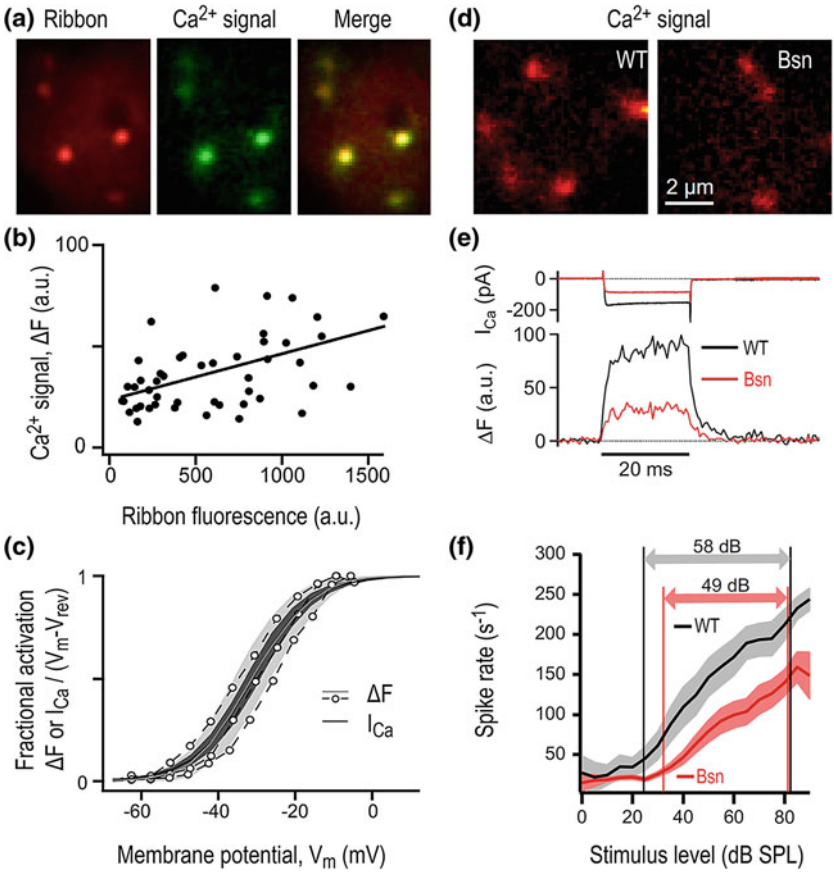

Fig. 5.7 Presynaptic Ca^{2+} influx and SGN response properties. **a** Live Ca^{2+} imaging with the indicator Fluo-5 N (*green*) and simultaneous detection of fluorescent ribbon binding peptide (*red*) demonstrates Ca^{2+} microdomains restricted to IHC AZs. **b** AZs with greater ribbon fluorescence (*x*-axis) tended to have more intense Ca^{2+} microdomain signals (*y*-axis). **c** Fractional activation of fluorescent Ca^{2+} signals by membrane potential illustrates heterogeneity in voltage dependence among AZs. *Open circles* connected by *dashed lines* show voltage activation of Ca^{2+} fluorescence for three individual AZs in one IHC. *Dark shaded area* is mean ± SD for the whole-cell Ca^{2+} current across cells; *light shaded area* is mean ± SD for synaptic Ca^{2+} microdomain fluorescence changes across AZs. **d** In bassoon-deficient IHCs (Bsn, *right*) Ca^{2+} microdomains were less intense than in wild-type (WT, *left*). **e** *Upper*, individual traces of whole-cell Ca^{2+} current in WT (*black*) and Bsn mouse IHCs (*red*). *Lower*, single AZ fluorescence changes indicate greater Ca^{2+} influx in WT. **f** AP rate versus sound pressure level for SGN recordings in vivo in WT (*black*) or Bsn (*red*). Solid lines are means across cells and shaded areas are ± SD. WT SGNs have greater SRs, steeper slopes, and larger dynamic ranges (10–90 % of maximum AP rate indicates dynamic range by *vertical lines*. (**a**–**c** adapted from Frank et al. 2009. Mechanisms contributing to synaptic Ca^{2+} signals and their heterogeneity in hair cells. *Proceedings of the National Academy of Sciences of the USA*, 106(11), 4483–4488. **d**, **e** adapted from Frank et al. 2010. Bassoon and the synaptic ribbon organize Ca^{2+} channels and vesicles to add release sites and promote refilling. *Neuron*, 68 (4), 724–738. **f** adapted from Wong et al. 2013. Concurrent maturation of inner hair cell synaptic Ca^{2+} influx and auditory nerve spontaneous activity around hearing onset in mice. *The Journal of Neuroscience*, 33(26), 10661–10666)

presynaptic and Ca^{2+} dependent (Goutman & Glowatzki, 2011; Goutman, 2012), suggesting that differences between IHC AZs contribute directly to the diversity observed in SGN firing properties.

Even without significant differences in postsynaptic efficacy of the SGNs innervating one IHC, diversity of SGN SRs might arise from heterogeneity in the presynaptic rate of release events (the EPSC rate). Curiously, when high- and low-SR synapses of the cat were compared quantitatively, the presynaptic ribbon sizes and vesicle numbers were similar (Kantardzhieva et al., 2013), suggesting that unseen presynaptic differences or postsynaptic neuron-intrinsic differences might influence SGN response diversity.

5.5.3 Postsynaptic Heterogeneity

Comparatively little is known about how rates of glutamate-evoked APs may be modulated by SGN-intrinsic mechanisms, either over time or among a population of SGNs. This section reviews observations in whole animals and in organ of Corti explants. Other SGN endogenous properties are covered in Chap. 4 by Davis and Crozier.

In some mammals, synapses of SGNs with different SRs can be distinguished by their size, morphology, and location on the IHC (Liberman, 1982). High-SR SGNs tended to innervate the pillar faces of IHCs, where synaptic ribbons were smaller (Liberman, 1980). The fibers of high-SR SGNs were also thicker, with greater mitochondrial content than fibers of low-SR SGNs. Like the larger mammals mainly used in studies of auditory nerve fiber physiology in vivo—cats, guinea pigs, gerbils, and chinchillas—mice also have SGNs with diverse firing properties (Taberner & Liberman, 2005) and AZs with heterogeneous morphologies (Meyer et al., 2009; Liberman et al., 2011). It remains to be determined if SGNs segregate around the IHC circumference according to SR and sensitivity in mice and humans, as they do in cats.

Species differences have been reported. For example in the gerbil, in contrast to the guinea pig and cat, differences between SGN terminal thicknesses were not seen around the IHC perimeter (Slepecky et al., 2000).

Among SGNs, potential mechanisms for diversity of excitability are postsynaptic heterogeneities of synaptic strength and AP generation. In this scenario, SGNs might be expected to vary markedly in the level of input required to evoke an EPSC of equivalent size or an AP of equivalent latency. The same concentration of glutamate in the cleft might produce EPSCs of different sizes in different SGNs. A variable-amplitude train of EPSCs might evoke high AP rates in one SGN but low rates in another.

On postsynaptic boutons in the mouse, immunohistochemistry with an antibody to AMPAR subunits GluA2/3 demonstrated that SGN boutons innervating the pillar faces of IHCs had larger immunoreactivity than those innervating the modiolar sides (Liberman et al., 2011), congruent with pillar SGNs corresponding to high-SR

fibers. Immunolabeled glutamate receptor clusters appear to vary significantly in overall intensity between SGN postsynaptic boutons (Meyer et al., 2009; Jing et al., 2013). However, the relationships among postsynaptic AMPAR expression, presynaptic $Ca_V1.3$ expression, and Ca^{2+}-microdomain amplitude as a function of synapse position within IHCs are not yet clear.

5.6 Summary and Conclusion

Deciphering the pre- and postsynaptic mechanisms of synaptic transmission at the hair cell ribbon synapse, the first afferent synapse in the auditory system, is essential for understanding how sound is encoded. We are only beginning to comprehend the molecular anatomy and physiology of the hair cell ribbon synapse, but it has become evident that it differs from that of a conventional CNS synapse. Synaptic specializations between a single IHC AZ and a single SGN PSD enable them to achieve unparalleled performance in terms of sustained high rates of temporally precise synaptic communication. Synaptic ribbons and associated scaffolds promote a large complement of presynaptic Ca^{2+} channels and fusion-competent vesicles that are likely to be molecularly coupled in a nanodomain signaling regime. Heterogeneity of Ca^{2+} channel number and properties among AZs seems essential for the synaptic diversity that enables decomposition of auditory information into functionally distinct SGNs. The fusion machinery still largely awaits discovery but involves unconventional and IHC-specific proteins such as the C_2 domain protein otoferlin, which is required for vesicle fusion and replenishment. The SGN efficiently turns presynaptic glutamate release into APs via sensitive glutamate detection tightly coupled with AP generation. Before attaining its mature structure and function as sound receiver in hearing animals, the hair cell synapse is active during development to provide presensory activity important for formation of the central auditory pathway.

Acknowledgments This work was supported by the Department of Otolaryngology at Washington University in St. Louis (M. A. R.) and a grant of the Deutsche Forschungsgemeinschaft to T. M. through the Collaborative Research Center 889.

References

Augustine, G. J., Adler, E. M., & Charltonc, M. P. (1991). The calcium signal for transmitter secretion from presynaptic nerve terminals. *Annals of the New York Academy of Sciences*, 635 (1), 365–381.

Baig, S. M., Koschak, A., Lieb, A., Gebhart, M., Dafinger, C., Nürnberg, G., Ali, A., Ahmad, I., Sinnegger-Brauns, M. J., & Brandt, N. (2011). Loss of CaV1. 3 (CACNA1D) function in a human channelopathy with bradycardia and congenital deafness. *Nature Neuroscience*, 14(1), 77–84.

Barnes, S., & Hille, B. (1989). Ionic channels of the inner segment of tiger salamander cone photoreceptors. *The Journal of General Physiology (JGP)*, 94(4), 719–743.

Beurg, M., Michalski, N., Safieddine, S., Bouleau, Y., Schneggenburger, R., Chapman, E. R., Petit, C., & Dulon, D. (2010). Control of exocytosis by synaptotagmins and otoferlin in auditory hair cells. *The Journal of Neuroscience*, 30(40), 13281–13290.

Beutner, D., & Moser, T. (2001). The presynaptic function of mouse cochlear inner hair cells during development of hearing. *The Journal of Neuroscience*, 21(13), 4593–4599.

Beutner, D., Voets, T., Neher, E., & Moser, T. (2001). Calcium dependence of exocytosis and endocytosis at the cochlear inner hair cell afferent synapse. *Neuron*, 29(3), 681–690.

Bohne, B. A., Kenworthy, A., & Carr, C. D. (1982). Density of myelinated nerve fibers in the chinchilla cochlea. *The Journal of the Acoustical Society of America*, 72(1), 102–107.

Brandt, A., Khimich, D., & Moser, T. (2005). Few CaV1.3 channels regulate the exocytosis of a synaptic vesicle at the hair cell ribbon synapse. *The Journal of Neuroscience*, 25(50), 11577–11585.

Brandt, A., Striessnig, J., & Moser, T. (2003). CaV1.3 channels are essential for development and presynaptic activity of cochlear inner hair cells. *The Journal of Neuroscience*, 23(34), 10832–10840.

Buran, B. N., Strenzke, N., Neef, A., Gundelfinger, E. D., Moser, T., & Liberman, M. C. (2010). Onset coding is degraded in auditory nerve fibers from mutant mice lacking synaptic ribbons. *The Journal of Neuroscience*, 30(22), 7587–7597.

Chapochnikov, N. M., Takago, H., Huang, C. H., Pangršič, T., Khimich, D., Neef, J., Auge, E., Göttfert, F., Hell, S. W., Wichmann, C., Wolf, F., & Moser, T. (2014). Uniquantal release through a dynamic fusion pore is a candidate mechanism of hair cell exocytosis. *Neuron*, 83(6), 1389–1403.

Cho, S., Li, G. L., & von Gersdorff, H. (2011). Recovery from short-term depression and facilitation is ultrafast and Ca^{2+}-dependent at auditory hair cell synapses. *The Journal of Neuroscience*, 31(15), 5682–5692.

Clause, A., Kim, G., Sonntag, M., Weisz, C. J. C., Vetter, D. E., Rűbsamen, R., & Kandler, K. (2014). The precise temporal pattern of prehearing spontaneous activity is necessary for tonotopic map refinement. *Neuron*, 82(4), 822–835.

Corey, D. P., & Hudspeth, A. J. (1979). Ionic basis of the receptor potential in a vertebrate hair cell. *Nature*, 281(5733), 675–677.

Cui, G., Meyer, A. C., Calin-Jageman, I., Neef, J., Haeseleer, F., Moser, T., & Lee, A. (2007). Ca^{2+}-binding proteins tune Ca^{2+}-feedback to CaV1.3 channels in mouse auditory hair cells. *The Journal of Physiology*, 585(3), 791–803.

Dallos, P. (1985). Response characteristics of mammalian cochlear hair cells. *The Journal of Neuroscience*, 5(6), 1591–1608.

Derbyshire, A. J., & Davis, H. (1935). The action potentials of the auditory nerve. Boston, MA: Department of Physiology, Harvard Medical School.

Dou, H., Vazquez, A. E., Namkung, Y., Chu, H., Cardell, E. L., Nie, L., Parson, S., Shin, H. S., & Yamoah, E. N. (2004). Null mutation of α1D Ca^{2+} channel gene results in deafness but no vestibular defect in mice. *Journal of the Association for Research in Otolaryngology (JARO)*, 5 (2), 215–226.

Duncker, S. V., Franz, C., Kuhn, S., Schulte, U., Campanelli, D., Brandt, N., Hirt, B., Fakler, B., Blin, N., & Ruth, P. (2013). Otoferlin couples to clathrin-mediated endocytosis in mature cochlear inner hair cells. *The Journal of Neuroscience*, 33(22), 9508–9519.

Ehret, G. (1976). Development of absolute auditory thresholds in the house mouse (*mus musculus*). *Ear and Hearing*, 1(5), 179–184.

Farris, H. E., Wells, G. B., & Ricci, A. J. (2006). Steady-state adaptation of mechanotransduction modulates the resting potential of auditory hair cells, providing an assay for endolymph [Ca^{2+}]. *The Journal of Neuroscience*, 26(48), 12526–12536.

Frank, T., Khimich, D., Neef, A., & Moser, T. (2009). Mechanisms contributing to synaptic Ca^{2+} signals and their heterogeneity in hair cells. *Proceedings of the National Academy of Sciences of the USA*, 106(11), 4483–4488.

Frank, T., Rutherford, M. A., Strenzke, N., Neef, A., Pangršič, T., Khimich, D., Fejtova, A., Gundelfinger, E. D., Liberman, M. C., Harke, B., Bryan, K. E., Lee, A., Egner, A., Riedel, D., & Moser, T. (2010). Bassoon and the synaptic ribbon organize Ca^{2+} channels and vesicles to add release sites and promote refilling. *Neuron*, 68(4), 724–738.

Fuchs, P. A. (2005). Time and intensity coding at the hair cell's ribbon synapse. *The Journal of Physiology*, 566(1), 7–12.

Fuchs, P. A., Evans, M. G., & Murrow, B. W. (1990). Calcium currents in hair cells isolated from the cochlea of the chick. *The Journal of Physiology*, 429(1), 553–568.

Furukawa, T., & Matsuura, S. (1978). Adaptive rundown of excitatory post-synaptic potentials at synapses between hair cells and eight nerve fibres in the goldfish. *The Journal of Physiology*, 276(1), 193–209.

Furukawa, T., Kuno, M., & Matsuura, S. (1982). Quantal analysis of a decremental response at hair cell-afferent fibre synapses in the goldfish sacculus. *The Journal of Physiology*, 322(1), 181–195.

Galambos, R., & Davis, H. (1944). *The response of single auditory-nerve fibers to acoustic stimulation*. Boston, MA: Department of Physiology, Harvard Medical School.

Gebhart, M., Juhasz-Vedres, G., Zuccotti, A., Brandt, N., Engel, J., Trockenbacher, A., Kaur, G., Obermair, G. J., Knipper, M., Koschak, A., & Striessnig, J. (2010). Modulation of cav1.3 ca2+ channel gating by rab3 interacting molecule. *Molecular and Cellular Neuroscience*, 44(3), 246–259.

Géléoc, G. S., & Holt, J. R. (2003). Auditory amplification: Outer hair cells *pres* the issue. *Trends in Neurosciences*, 26(3), 115–117.

Glowatzki, E., & Fuchs, P. A. (2000). Cholinergic synaptic inhibition of inner hair cells in the neonatal mammalian cochlea. *Science*, 288(5475), 2366–2368.

Glowatzki, E., & Fuchs, P. A. (2002). Transmitter release at the hair cell ribbon synapse. *Nature Neuroscience*, 5(2), 147–154.

Goutman, J. D. (2012). Transmitter release from cochlear hair cells is phase locked to cyclic stimuli of different intensities and frequencies. *The Journal of Neuroscience*, 32(47), 17025–17036.

Goutman, J. D., & Glowatzki, E. (2007). Time course and calcium dependence of transmitter release at a single ribbon synapse. *Proceedings of the National Academy of Sciences of the USA*, 104(41), 16341–16346.

Goutman, J. D., & Glowatzki, E. (2011). Short-term facilitation modulates size and timing of the synaptic response at the inner hair cell ribbon synapse. *The Journal of Neuroscience*, 31(22), 7974–7981.

Grant, L., & Fuchs, P. (2008). Calcium-and calmodulin-dependent inactivation of calcium channels in inner hair cells of the rat cochlea. *The Journal of Neurophysiology*, 99(5), 2183–2193.

Grant, L., Yi, E., & Glowatzki, E. (2010). Two modes of release shape the postsynaptic response at the inner hair cell ribbon synapse. *The Journal of Neuroscience*, 30(12), 4210–4220.

Graydon, C. W., Cho, S., Li, G. L., Kachar, B., & von Gersdorff, H. (2011). Sharp Ca^{2+} nanodomains beneath the ribbon promote highly synchronous multivesicular release at hair cell synapses. *The Journal of Neuroscience*, 31(46), 16637–16650.

Gregory, F. D., Bryan, K. E., Pangršič, T., Calin-Jageman, I. E., Moser, T., & Lee, A. (2011). Harmonin inhibits presynaptic CaV1.3 Ca^{2+} channels in mouse inner hair cells. *Nature Neuroscience*, 14(9), 1109–1111.

Heidelberger, R., & Matthews, G. (1992). Calcium influx and calcium current in single synaptic terminals of goldfish retinal bipolar neurons. *The Journal of Physiology*, 447(1), 235–256.

Heil, P., & Irvine, D. R. (1997). First-spike timing of auditory-nerve fibers and comparison with auditory cortex. *Journal of Neurophysiology*, 78(5), 2438–2454.

Heil, P., & Neubauer, H. (2001). Temporal integration of sound pressure determines thresholds of auditory-nerve fibers. *The Journal of Neuroscience*, 21(18), 7404–7415.

Heil, P., & Neubauer, H. (2003). A unifying basis of auditory thresholds based on temporal summation. *Proceedings of the National Academy of Sciences of the USA*, 100(10), 6151–6156.

Heil, P., & Neubauer, H. (2010). Summing across different active zones can explain the quasi-linear Ca^{2+}-dependencies of exocytosis by receptor cells. *Frontiers in Synaptic Neuroscience*, 2.

Hibino, H., Pironkova, R., Onwumere, O., Vologodskaia, M., Hudspeth, A. J., & Lesage, F. (2002). Rim binding proteins (RBPs) couple rab3-interacting molecules (RIMs) to voltage-gated Ca^{2+} channels. *Neuron*, 34(3), 411–423.

Hossain, W. A., Antic, S. D., Yang, Y., Rasband, M. N., & Morest, D. K. (2005). Where is the spike generator of the cochlear nerve? Voltage-gated sodium channels in the mouse cochlea. *The Journal of Neuroscience*, 25(29), 6857–6868.

Huang, L. C., Thorne, P. R., Housley, G. D., & Montgomery, J. M. (2007). Spatiotemporal definition of neurite outgrowth, refinement and retraction in the developing mouse cochlea. *Development*, 134(16), 2925–2933.

Huang, L. C., Barclay, M., Lee, K., Peter, S., Housley, G. D., Thorne, P. R., Montgomery, J. M., & others (2012). Synaptic profiles during neurite extension, refinement and retraction in the developing cochlea. *Neural Development*, 7 1–17.

Hudspeth, A. J., & Lewis, R. S. (1988). Kinetic analysis of voltage-and ion-dependent conductances in saccular hair cells of the bull-frog, *rana catesbeiana*. *The Journal of Physiology*, 400(1), 237–274.

Issa, N. P., & Hudspeth, A. J. (1996). The entry and clearance of Ca^{2+} at individual presynaptic active zones of hair cells from the bullfrog's sacculus. *Proceedings of the National Academy of Sciences of the USA*, 93(18), 9527–9532.

Jing, Z., Rutherford, M. A., Takago, H., Frank, T., Fejtova, A., Khimich, D., Moser, T., & Strenzke, N. (2013). Disruption of the presynaptic cytomatrix protein bassoon degrades ribbon anchorage, multiquantal release, and sound encoding at the hair cell afferent synapse. *The Journal of Neuroscience*, 33(10), 4456–4467.

Johnson, S. L., Marcotti, W., & Kros, C. J. (2005). Increase in efficiency and reduction in Ca^{2+} dependence of exocytosis during development of mouse inner hair cells. *The Journal of Physiology*, 563(1), 177–191.

Johnson, S. L., Forge, A., Knipper, M., Munkner, S., & Marcotti, W. (2008). Tonotopic variation in the calcium dependence of neurotransmitter release and vesicle pool replenishment at mammalian auditory ribbon synapses. *The Journal of Neuroscience*, 28(30), 7670–7678.

Johnson, S. L., Franz, C., Kuhn, S., Furness, D. N., Rüttiger, L., Münkner, S., Rivolta, M. N., Seward, E. P., Herschman, H. R., & Engel, J. (2010). Synaptotagmin IV determines the linear Ca^{2+} dependence of vesicle fusion at auditory ribbon synapses. *Nature Neuroscience*, 13(1), 45–52.

Johnson, S. L., Eckrich, T., Kuhn, S., Zampini, V., Franz, C., Ranatunga, K. M., Roberts, T. P., Masetto, S., Knipper, M., Kros, C. J., & Marcotti, W. (2011). Position-dependent patterning of spontaneous action potentials in immature cochlear inner hair cells. *Nature Neuroscience*, 14 (6), 711–717.

Kaeser, P. S., Deng, L., Wang, Y., Dulubova, I., Liu, X., Rizo, J., & Südhof, T. C. (2011). RIM proteins tether Ca^{2+} channels to presynaptic active zones via a direct PDZ-domain interaction. *Cell*, 144(2), 282–295.

Kantardzhieva, A., Peppi, M., Lane, W. S., & Sewell, W. F. (2012). Protein composition of immunoprecipitated synaptic ribbons. *Journal of Proteome Research*, 11(2), 1163–1174.

Kantardzhieva, A., Liberman, M. C., & Sewell, W. F. (2013). Quantitative analysis of ribbons, vesicles, and cisterns at the cat inner hair cell synapse: Correlations with spontaneous rate: hair cell synaptic ribbons. *Journal of Comparative Neurology*, 521(14), 3260–3271.

Keen, E. C., & Hudspeth, A. J. (2006). Transfer characteristics of the hair cell's afferent synapse. *Proceedings of the National Academy of Sciences of the USA*, 103(14), 5537–5542.

Khimich, D., Nouvian, R., Pujol, R., tom Dieck, S., Egner, A., Gundelfinger, E. D., and Moser, T. (2005). Hair cell synaptic ribbons are essential for synchronous auditory signalling. *Nature*, 434, 889–894.

Kiang, N. Y. S. (1965). *Discharge patterns of single fibers in the cat's auditory nerve*. Cambridge, MA: MIT Press.

Kim, M. H., Li, G. L., & von Gersdorff, H. (2013). Single Ca^{2+} channels and exocytosis at sensory synapses. *The Journal of Physiology*, 591(13), 3167–3178.

Knudsen, E. I., & Konishi, M. (1979). Mechanisms of sound localization in the barn owl (*tyto alba*). *Journal of Comparative Physiology*, 133(1), 13–21.

Koschak, A., Reimer, D., Huber, I., Grabner, M., Glossmann, H., Engel, J., & Striessnig, J. (2001). Alpha 1D (CaV1. 3) subunits can form L-type Ca^{2+} channels activating at negative voltages. *The Journal of Biological Chemistry (jbc)*, 276(25), 22100–22106.

Kros, C. J., Ruppersberg, J. P., & Rüsch, A. (1998). Expression of a potassium current in inner hair cells during development of hearing in mice. *Nature*, 394(6690), 281–284.

Kubisch, C., Schroeder, B. C., Friedrich, T., Lütjohann, B., El-Amraoui, A., Marlin, S., Petit, C., & Jentsch, T. J. (1999). KCNQ4, a novel potassium channel expressed in sensory outer hair cells, is mutated in dominant deafness. *Cell*, 96(3), 437–446.

Lacas-Gervais, S., Guo, J., Strenzke, N., Scarfone, E., Kolpe, M., Jahkel, M., De Camilli, P., Moser, T., Rasband, M. N., Solimena, M. (2004). βIVΣ1 spectrin stabilizes the nodes of Ranvier and axon initial segments. *The Journal of Cell Biology (JCB)*, 166(7), 983–990.

Lee, A., Scheuer, T., & Catterall, W. A. (2000). Ca^{2+}/calmodulin-dependent facilitation and inactivation of P/Q-type Ca^{2+} channels. *The Journal of Neuroscience*, 20(18), 6830–6838.

Lenoir, M., Shnerson, A., & Pujol, R. (1980). Cochlear receptor development in the rat with emphasis on synaptogenesis. *Anatomy and Embryology*, 160(3), 253–262.

Lenzi, D., & von Gersdorff, H. (2001). Structure suggests function: The case for synaptic ribbons as exocytotic nanomachines. *Bioessays*, 23(9), 831–840.

Lenzi, D., Crum, J., Ellisman, M. H., & Roberts, W. M. (2002). Depolarization redistributes synaptic membrane and creates a gradient of vesicles on the synaptic body at a ribbon synapse. *Neuron*, 36(4), 649–659.

Li, G. L., Keen, E., Andor-Ardo, D., Hudspeth, A. J., & von Gersdorff, H. (2009). The unitary event underlying multiquantal EPSCs at a hair cell's ribbon synapse. *The Journal of Neuroscience*, 29(23), 7558–7568.

Li, G. L., Cho, S., & von Gersdorff, H. (2014). Phase-locking precision is enhanced by multiquantal release at an auditory hair cell ribbon synapse. *Neuron*, 83(6), 1404–1417.

Liberman, M. C. (1978). Auditory-nerve response from cats raised in a low-noise chamber. *The Journal of the Acoustical Society of America*, 63(2), 442–455.

Liberman, M. C. (1980). Morphological differences among radial afferent fibers in the cat cochlea: An electron-microscopic study of serial sections. *Hearing Research*, 3(1), 45–63.

Liberman, M. C. (1982). Single-neuron labeling in the cat auditory nerve. *Science*, 216(4551), 1239–1241.

Liberman, L. D., Wang, H., & Liberman, M. C. (2011). Opposing gradients of ribbon size and AMPA receptor expression underlie sensitivity differences among cochlear-nerve/hair-cell synapses. *The Journal of Neuroscience*, 31(3), 801–808.

Lysakowski, A., Gaboyard-Niay, S., Calin-Jageman, I., Chatlani, S., Price, S. D., & Eatock, R. A. (2011). Molecular microdomains in a sensory terminal, the vestibular calyx ending. *The Journal of Neuroscience*, 31(27), 10101–10114.

Magupalli, V. G., Schwarz, K., Alpadi, K., Natarajan, S., Seigel, G. M., & Schmitz, F. (2008). Multiple ribeye-ribeye interactions create a dynamic scaffold for the formation of synaptic ribbons. *The Journal of Neuroscience*, 28(32), 7954–7967.

Marcotti, W., Johnson, S. L., Rusch, A., & Kros, C. J. (2003). Sodium and calcium currents shape action potentials in immature mouse inner hair cells. *The Journal of Physiology*, 552(3), 743–761.

Martinez-Dunst, C., Michaels, R. L., & Fuchs, P. A. (1997). Release sites and calcium channels in hair cells of the chick's cochlea. *The Journal of Neuroscience*, 17(23), 9133–9144.

Matthews, G., & Fuchs, P. (2010). The diverse roles of ribbon synapses in sensory neurotransmission. *Nature Reviews Neuroscience*, 11(12), 812–822.

Matveev, V., Bertram, R., & Sherman, A. (2011). Calcium cooperativity of exocytosis as a measure of Ca^{2+} channel domain overlap. *Brain Research*, 1398 126–138.

Meddis, R. (2006). Auditory-nerve first-spike latency and auditory absolute threshold: A computer model. *The Journal of the Acoustical Society of America*, 119(1), 406–417.

Merchan-Perez, A., & Liberman, M. C. (1996). Ultrastructural differences among afferent synapses on cochlear hair cells: Correlations with spontaneous discharge rate. *Journal of Comparative Neurology*, 371(2), 208–221.

Meyer, A. C., Frank, T., Khimich, D., Hoch, G., Riedel, D., Chapochnikov, N. M., Yarin, Y. M., Harke, B., Hell, S. W., Egner, A., & Moser, T. (2009). Tuning of synapse number, structure and function in the cochlea. *Nature Neuroscience*, 12(4), 444–453.

Moser, T., & Beutner, D. (2000). Kinetics of exocytosis and endocytosis at the cochlear inner hair cell afferent synapse of the mouse. *Proceedings of the National Academy of Sciences of the USA*, 97(2), 883–888.

Moser, T., Neef, A., & Khimich, D. (2006). Mechanisms underlying the temporal precision of sound coding at the inner hair cell ribbon synapse. *The Journal of Physiology*, 576(1), 55–62.

Neef, J., Gehrt, A., Bulankina, A. V., Meyer, A. C., Riedel, D., Gregg, R. G., Strenzke, N., & Moser, T. (2009). The Ca^{2+} channel subunit β2 regulates Ca^{2+} channel abundance and function in inner hair cells and is required for hearing. *The Journal of Neuroscience*, 29(34), 10730–10740.

Neef, J., Jung, S., Wong, A. B., Reuter, K., Pangrsic, T., Chakrabarti, R., Kugler, S., Lenz, C., Nouvian, R., Boumil, R. M., Frankel, W. N., Wichmann, C., & Moser, T. (2014). Modes and regulation of endocytic membrane retrieval in mouse auditory hair cells. *The Journal of Neuroscience*, 34(3), 705–716.

Nouvian, R., Beutner, D., Parsons, T. D., & Moser, T. (2006). Structure and function of the hair cell ribbon synapse. *Journal of Membrane Biology*, 209(2–3), 153–165.

Nouvian, R., Neef, J., Bulankina, A. V., Reisinger, E., Pangršič, T., Frank, T., Sikorra, S., Brose, N., Binz, T., & Moser, T. (2011). Exocytosis at the hair cell ribbon synapse apparently operates without neuronal snare proteins. *Nature Neuroscience*, 14(4), 411–413.

Nusser, Z., Lujan, R., Laube, G., Roberts, J. D. B., Molnar, E., & Somogyi, P. (1998). Cell type and pathway dependence of synaptic AMPA receptor number and variability in the hippocampus. *Neuron*, *21*(3), 545–559.

Ohlemiller, K. K., Echteler, S. M., & Siegel, J. H. (1991). Factors that influence rate-versus-intensity relations in single cochlear nerve fibers of the gerbil. *The Journal of the Acoustical Society of America*, 90(1), 274–287.

Oliver, D., Knipper, M., Derst, C., & Fakler, B. (2003). Resting potential and submembrane calcium concentration of inner hair cells in the isolated mouse cochlea are set by KCNQ-type potassium channels. *The Journal of Neuroscience*, 23(6), 2141–2149.

Oliver, D., Taberner, A. M., Thurm, H., Sausbier, M., Arntz, C., Ruth, P., Fakler, B., & Liberman, M. C. (2006). The role of BK_{Ca} channels in electrical signal encoding in the mammalian auditory periphery. *The Journal of Neuroscience*, 26(23), 6181–6189.

Palmer, A. R., & Russell, I. J. (1986). Phase-locking in the cochlear nerve of the guinea-pig and its relation to the receptor potential of inner hair cells. *Hearing Research*, 24(1), 1–15.

Pangršič, T., Lasarow, L., Reuter, K., Takago, H., Schwander, M., Riedel, D., Frank, T., Tarantino, L. M., Bailey, J. S., Strenzke, N., Brose, N., Müller, U., Reisinger, E., & Moser, T. (2010). Hearing requires otoferlin-dependent efficient replenishment of synaptic vesicles in hair cells. *Nature Neuroscience*, 13(7), 869–876.

Parsons, T. D., Lenzi, D., Almers, W., & Roberts, W. M. (1994). Calcium-triggered exocytosis and endocytosis in an isolated presynaptic cell: Capacitance measurements in saccular hair cells. *Neuron*, 13(4), 875–883.

Platzer, J., Engel, J., Schrott-Fischer, A., Stephan, K., Bova, S., Chen, H., Zheng, H., & Striessnig, J. (2000). Congenital deafness and sinoatrial node dysfunction in mice lacking class D L-type Ca^{2+} channels. *Cell*, 102(1), 89–97.

Ramakrishnan, N. A., Drescher, M. J., & Drescher, D. G. (2009). Direct interaction of otoferlin with syntaxin 1a, SNAP-25, and the L-type voltage-gated calcium channel CaV1.3. *The Journal of Biological Chemistry (jbc)*, 284(3), 1364–1372.

Raman, I. M., Sprunger, L. K., Meisler, M. H., & Bean, B. P. (1997). Altered subthreshold sodium currents and disrupted firing patterns in purkinje neurons of *SCN8A* mutant mice. *Neuron*, 19 (4), 881–891.

Reisinger, E., Bresee, C., Neef, J., Nair, R., Reuter, K., Bulankina, A., Nouvian, R., Koch, M., Buckers, J., Kastrup, L., Roux, I., Petit, C., Hell, S. W., Brose, N., Rhee, J. S., Kugler, S., Brigande, J. V., & Moser, T. (2011). Probing the functional equivalence of otoferlin and synaptotagmin 1 in exocytosis. *The Journal of Neuroscience*, 31(13), 4886–4895.

Relkin, E. M., & Doucet, J. R. (1991). Recovery from prior stimulation. I: Relationship to spontaneous firing rates of primary auditory neurons. *Hearing Research*, 55(2), 215–222.

Roberts, W. M. (1993). Spatial calcium buffering in saccular hair cells. *Nature*, 363, 74–76.

Roberts, W. M., Jacobs, R. A., & Hudspeth, A. J. (1990). Colocalization of ion channels involved in frequency selectivity and synaptic transmission at presynaptic active zones of hair cells. *The Journal of Neuroscience*, 10(11), 3664–3684.

Robertson, D., & Paki, B. (2002). Role of L-type Ca^{2+} channels in transmitter release from mammalian inner hair cells. II. Single-neuron activity. *Journal of Neurophysiology*, 87(6), 2734–2740.

Rodriguez-Contreras, A., & Yamoah, E. N. (2001). Direct measurement of single-channel Ca^{2+} currents in bullfrog hair cells reveals two distinct channel subtypes. *The Journal of Physiology*, 534(3), 669–689.

Rose, J. E., Brugge, J. F., Anderson, D. J., Hind, J. E., & others (1967). Phase-locked response to low-frequency tones in single auditory nerve fibers of the squirrel monkey. *Journal of Neurophysiology*, 30(4), 769–793.

Roux, I., Safieddine, S., Nouvian, R., Simmler, M. C., Bahloul, A., Perfettini, I., Le Gall, M., Rostaing, P., Hamard, G., & Triller, A. (2006). Otoferlin, defective in a human deafness form, is essential for exocytosis at the auditory ribbon synapse. *Cell*, 127(2), 277–289.

Ruel, J., Nouvian, R., d' Aldin, C. G., Pujol, R., Eybalin, M., & Puel, J. L. (2001). Dopamine inhibition of auditory nerve activity in the adult mammalian cochlea. *European Journal of Neuroscience*, 14(6), 977–986.

Ruel, J., Emery, S., Nouvian, R., Bersot, T., Amilhon, B., Van Rybroek, J. M., Rebillard, G., Lenoir, M., Eybalin, M., Delprat, B., Sivakumaran, T. A., Giros, B., El Mestikawy, S., Moser, T., Smith, R. J. H., Lesperance, M. M., & Puel, J. L. (2008). Impairment of SLC17A8 encoding vesicular glutamate transporter-3, VGLUT3, underlies nonsyndromic deafness DFNA25 and inner hair cell dysfunction in null mice. *The American Journal of Human Genetics*, 83(2), 278–292.

Rüsch, A., Ng, L., Goodyear, R., Oliver, D., Lisoukov, I., Vennström, B., Richardson, G., Kelley, M. W., & Forrest, D. (2001). Retardation of cochlear maturation and impaired hair cell function caused by deletion of all known thyroid hormone receptors. *The Journal of Neuroscience*, 21(24), 9792–9800.

Russell, I. J., & Sellick, P. M. (1978). Intracellular studies of hair cells in the mammalian cochlea. *The Journal of Physiology*, 284(1), 261–290.

Rutherford, M. A., & Pangršič, T. (2012). Molecular anatomy and physiology of exocytosis in sensory hair cells. *Cell Calcium*, 52(3), 327–337.

Rutherford, M. A., Chapochnikov, N. M., & Moser, T. (2012). Spike encoding of neurotransmitter release timing by spiral ganglion neurons of the cochlea. *The Journal of Neuroscience*, 32(14), 4773–4789.

Rutherford, M. A. (2015). Resolving the structure of inner ear ribbon synapses with STED microscopy. *Synapse*, 69(5), 242-255.

Sachs, M. B., Winslow, R. L., & Sokolowski, B. H. (1989). A computational model for rate-level functions from cat auditory-nerve fibers. *Hearing Research*, 41(1), 61–69.

Safieddine, S., & Wenthold, R. J. (1999). SNARE complex at the ribbon synapses of cochlear hair cells: Analysis of synaptic vesicle-and synaptic membrane-associated proteins. *European Journal of Neuroscience*, 11(3), 803–812.

Saito, K. (1990). Freeze-fracture organization of hair cell synapses in the sensory epithelium of guinea pig organ of corti. *Journal of Electron Microscopy Technique*, 15(2), 173–186.

Santos-Sacchi, J. (1993). Voltage-dependent ionic conductances of type I spiral ganglion cells from the guinea pig inner ear. *The Journal of Neuroscience*, 13(8), 3599–3611.

Schmitz, F., Königstorfer, A., & Südhof, T. C. (2000). RIBEYE, a component of synaptic ribbons: A protein's journey through evolution provides insight into synaptic ribbon function. *Neuron*, 28(3), 857–872.

Schnee, M. E., Lawton, D. M., Furness, D. N., Benke, T. A., & Ricci, A. J. (2005). Auditory hair cell-afferent fiber synapses are specialized to operate at their best frequencies. *Neuron*, 47(2), 243–254.

Schnee, M. E., Castellano-Muñoz, M., & Ricci, A. J. (2013). Response properties from turtle auditory hair cell afferent fibers suggest spike generation is driven by synchronized release both between and within synapses. *Journal of Neurophysiology*, 110(1), 204–220.

Schrauwen, I., Helfmann, S., Inagaki, A., Predoehl, F., Tabatabaiefar, M. A., Picher, M. M., Sommen, M., Seco, C. Z., Oostrik, J., Kremer, H., Dheedene, A., Claes, C., Fransen, E., Chaleshtori, M. H., Coucke, P., Lee, A., Moser, T., & Van Camp, G. (2012). A mutation in CaBP2, expressed in cochlear hair cells, causes autosomal-recessive hearing impairment. *The American Journal of Human Genetics*, 91(4), 636–645.

Schwarz, K., Natarajan, S., Kassas, N., Vitale, N., & Schmitz, F. (2011). The synaptic ribbon is a site of phosphatidic acid generation in ribbon synapses. *The Journal of Neuroscience*, 31(44), 15996–16011.

Sendin, G., Bulankina, A. V., Riedel, D., & Moser, T. (2007). Maturation of ribbon synapses in hair cells is driven by thyroid hormone. *The Journal of Neuroscience*, 27(12), 3163–3173.

Sendin, G., Bourien, J., Rassendren, F., Puel, J. L., & Nouvian, R. (2014). Spatiotemporal pattern of action potential firing in developing inner hair cells of the mouse cochlea. *Proceedings of the National Academy of Sciences of the USA*, 111(5), 1999–2004.

Sewell, W. F. (1984). The relation between the endocochlear potential and spontaneous activity in auditory nerve fibres of the cat. *The Journal of Physiology*, 347(1), 685–696.

Sheets, L., Trapani, J. G., Mo, W., Obholzer, N., & Nicolson, T. (2011). Ribeye is required for presynaptic CaV1.3 channel localization and afferent innervation of sensory hair cells. *Development*, 138(7), 1309–1319.

Shnerson, A., Devigne, C., & Pujol, R. (1981). Age-related changes in the C57Bl/6j mouse cochlea. II. ultrastructural findings. *Developmental Brain Research*, 2(1), 77–88.

Siegel, J. H. (1992). Spontaneous synaptic potentials from afferent terminals in the guinea pig cochlea. *Hearing Research*, 59(1), 85–92.

Siegel, J. H., & Relkin, E. M. (1987). Antagonistic effects of perilymphatic calcium and magnesium on the activity of single cochlear afferent neurons. *Hearing Research*, 28(2), 131–147.

Slepecky, N. B., Galsky, M. D., Swartzentruber-Martin, H., & Savage, J. (2000). Study of afferent nerve terminals and fibers in the gerbil cochlea: Distribution by size. *Hearing Research*, 144 (1), 124–134.

Smith, C. A., & Sjöstrand, F. S. (1961). Structure of the nerve endings on the external hair cells of the guinea pig cochlea as studied by serial sections. *Journal of Ultrastructure Research*, 5(6), 523–556.

Sobkowicz, H. M., Rose, J. E., Scott, G. E., & Slapnick, S. M. (1982). Ribbon synapses in the developing intact and cultured organ of corti in the mouse. *The Journal of Neuroscience*, 2(7), 942–957.

Spassova, M., Eisen, M. D., Saunders, J. C., & Parsons, T. D. (2001). Chick cochlear hair cell exocytosis mediated by dihydropyridine-sensitive calcium channels. *The Journal of Physiology*, 535(3), 689–696.

Spassova, M. A., Avissar, M., Furman, A. C., Crumling, M. A., Saunders, J. C., & Parsons, T. D. (2004). Evidence that rapid vesicle replenishment of the synaptic ribbon mediates recovery from short-term adaptation at the hair cell afferent synapse. *Journal of the Association for Research in Otolaryngology*, 5(4), 376–390.

Spoendlin, H. (1972). Innervation densities of the cochlea. *Acta Oto-Laryngologica*, 73(2),–(6), 235–248.

Stevens, S. S., & Davis, H. (1938/1983). *Hearing: Its psychology and physiology.* American Institute of Physics for the Acoustical Society of America.

Strenzke, N., Chanda, S., Kopp-Scheinpflug, C., Khimich, D., Reim, K., Bulankina, A. V., Neef, A., Wolf, F., Brose, N., Xu-Friedman, M. A., & Moser, T. (2009). Complexin-I is required for high-fidelity transmission at the endbulb of held auditory synapse. *The Journal of Neuroscience*, 29(25), 7991–8004.

Taberner, A. M. & Liberman, M. C. (2005). Response properties of single auditory nerve fibers in the mouse. *Journal of Neurophysiology*, 93(1), 557–569.

Tachibana, M., Okada, T., Arimura, T., Kobayashi, K., & Piccolino, M. (1993). Dihydropyridine-sensitive calcium current mediates neurotransmitter release from bipolar cells of the goldfish retina. *The Journal of Neuroscience*, 13(7), 2898–2909.

Tritsch, N. X., & Bergles, D. E. (2010). Developmental regulation of spontaneous activity in the mammalian cochlea. *The Journal of Neuroscience*, 30(4), 1539–1550.

Tritsch, N. X., Yi, E., Gale, J. E., Glowatzki, E., & Bergles, D. E. (2007). The origin of spontaneous activity in the developing auditory system. *Nature*, 450(7166), 50–55.

Tucker, T., & Fettiplace, R. (1995). Confocal imaging of calcium microdomains and calcium extrusion in turtle hair cells. *Neuron*, 15(6), 1323–1335.

Uthaiah, R. C., & Hudspeth, A. J. (2010). Molecular anatomy of the hair cell's ribbon synapse. *The Journal of Neuroscience*, 30(37), 12387–12399.

Verpy, E., Leibovici, M., Zwaenepoel, I., Liu, X. Z., Gal, A., Salem, N., Mansour, A., Blanchard, S., Kobayashi, I., & Keats, B. J. (2000). A defect in harmonin, a PDZ domain-containing protein expressed in the inner ear sensory hair cells, underlies Usher syndrome type 1C. *Nature Genetics*, 26(1), 51–55.

Vincent, P. F. Y., Bouleau, Y., Safieddine, S., Petit, C., & Dulon, D. (2014). Exocytotic machineries of vestibular type I and cochlear ribbon synapses display similar intrinsic otoferlin-dependent Ca^{2+} sensitivity but a different coupling to Ca^{2+} channels. *The Journal of Neuroscience*, 34(33), 10853–10869.

Waites, C. L., Leal-Ortiz, S. A., Okerlund, N., Dalke, H., Fejtova, A., Altrock, W. D., Gundelfinger, E. D., & Garner, C. C. (2013). Bassoon and piccolo maintain synapse integrity by regulating protein ubiquitination and degradation. *The EMBO Journal*, 32(7), 954–969.

Walsh, E. J., & McGee, J. (1987). Postnatal development of auditory nerve and cochlear nucleus neuronal responses in kittens. *Hearing Research*, 28(1), 97–116.

Walsh, E. J., & Romand, R. (1992). Functional development of the cochlea and the cochlear nerve. *Development of Auditory and Vestibular Systems*, 2 161–219.

Walsh, B. T., Miller, J. B., Gacek, R., & Kiang, N. Y. S. (1972). Spontaneous activity in the eighth cranial nerve of the cat. *International Journal of Neuroscience*, 3(5), 221–235.

Weiss, T. F. (1966). A model of the peripheral auditory system. *Kybernetik*, 3(4), 153–175.

Wen, B., Wang, G. I., Dean, I., & Delgutte, B. (2009). Dynamic range adaptation to sound level statistics in the auditory nerve. *The Journal of Neuroscience*, 29(44), 13797–13808.

Westerman, L. A., & Smith, R. L. (1984). Rapid and short-term adaptation in auditory nerve responses. *Hearing Research*, 15(3), 249–260.

Wever, E. G., & Lawrence, M. (1954). *Physiological acoustics*. Princeton, NJ: Princeton University Press.

Winter, I. M., Robertson, D., & Yates, G. K. (1990). Diversity of characteristic frequency rate-intensity functions in guinea pig auditory nerve fibres. *Hearing Research*, 45(3), 191–202.

Wittig, J. H., & Parsons, T. D. (2008). Synaptic ribbon enables temporal precision of hair cell afferent synapse by increasing the number of readily releasable vesicles: A modeling study. *The Journal of Neurophysiology*, 100(4), 1724–1739.

Wong, A. B., Jing, Z., Rutherford, M. A., Frank, T., Strenzke, N., & Moser, T. (2013). Concurrent maturation of inner hair cell synaptic Ca^{2+} influx and auditory nerve spontaneous activity around hearing onset in mice. *The Journal of Neuroscience*, 33(26), 10661–10666.

Wong, A. B., Rutherford, M. A., Gabrielaitis, M., Pangršič, T., Göttfert, F., Frank, T., Michanski, S., Hell, S., Wolf, F., Wichmann, C., & Moser, T. (2014). Developmental refinement of hair cell synapses tightens the coupling of Ca $^{2+}$ influx to exocytosis. *The EMBO Journal*, 33(3), 247–264.

Wu, X. S., Xue, L., Mohan, R., Paradiso, K., Gillis, K. D., & Wu, L. G. (2007). The origin of quantal size variation: Vesicular glutamate concentration plays a significant role. *Journal of Neuroscience*, 27(11), 3046–3056.

Yang, P. S., Alseikhan, B. A., Hiel, H., Grant, L., Mori, M. X., Yang, W., Fuchs, P. A., & Yue, D. T. (2006). Switching of Ca^{2+}-dependent inactivation of CaV1.3 channels by calcium binding proteins of auditory hair cells. *The Journal of Neuroscience*, 26(42), 10677–10689.

Yasunaga, S., Grati, M., Cohen-Salmon, M., El-Amraoui, A., Mustapha, M., Salem, N., El-Zir, E., Loiselet, J., & Petit, C. (1999). A mutation in OTOF, encoding otoferlin, a FER-1-like protein, causes DFNB9, a nonsyndromic form of deafness. *Nature Genetics*, 21(4), 363–369.

Yi, E., Roux, I., & Glowatzki, E. (2010). Dendritic HCN channels shape excitatory postsynaptic potentials at the inner hair cell afferent synapse in the mammalian cochlea. *Journal of Neurophysiology*, 103(5), 2532–2543.

Zagaeski, M., Cody, A. R., Russell, I. J., & Mountain, D. C. (1994). Transfer characteristic of the inner hair cell synapse: Steady-state analysis. *The Journal of the Acoustical Society of America*, 95(6), 3430–3434.

Zampini, V., Johnson, S. L., Franz, C., Lawrence, N. D., Munkner, S., Engel, J., Knipper, M., Magistretti, J., Masetto, S., & Marcotti, W. (2010). Elementary properties of CaV1.3 Ca^{2+} channels expressed in mouse cochlear inner hair cells. *The Journal of Physiology*, 588(1), 187–199.

Zampini, V., Johnson, S. L., Franz, C., Knipper, M., Holley, M. C., Magistretti, J., Masetto, S., & Marcotti, W. (2013). Burst activity and ultrafast activation kinetics of CaV1.3 Ca^{2+} channels support presynaptic activity in adult gerbil hair cell ribbon synapses. *The Journal of Physiology*, 591(16), 3811–3820.

Zhang, S. Y., Robertson, D., Yates, G., & Everett, A. (1999). Role of L-type Ca^{2+} channels in transmitter release from mammalian inner hair cells I. Gross sound-evoked potentials. *Journal of Neurophysiology*, 82(6), 3307–3315.